Ocean Engineering 309 (2024) 118612

Contents lists available at ScienceDirect

Ocean Engineering

journal homepage: www.elsevier.com/locate/oceaneng

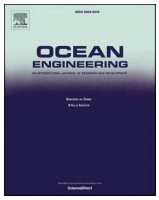

Research paper

Experimental modelling of a novel concrete-based 15-MW spar wind turbine

M. Somoano [a,b], P. Trubat [c], R. Guanche [a,*], C. Molins [c]

[a] IHCantabria - Instituto de Hidráulica Ambiental de La Universidad de Cantabria, Parque Científico y Tecnológico de Cantabria (PCTCAN), C/Isabel Torres 15, 39011, Santander, Spain
[b] Department of Construction and Manufacturing Engineering, Universidad de Oviedo, C/Pedro Puig Adam s/n, 33203, Gijón, Spain
[c] Analysis and Technology of Structures and Materials Group, Universitat Politècnica de Catalunya (UPC BarcelonaTech), C/Jordi Girona 1-3, 08034, Barcelona, Spain

ARTICLE INFO

Keywords:
Offshore wind turbine
Floating wind turbine
Spar wind turbine
Basin tests
Tank tests
Hybrid modelling

ABSTRACT

Physical model testing is a crucial step in the validation process of floating offshore wind concepts that can be used to contribute to the worldwide decarbonization objectives. It is also important to understand the coupled performance of all the sub-systems that conform to a floating wind concept: wind turbines, mooring systems or floating platform hydrodynamic responses. Few experimental tests had been conducted, and no real-time hybrid modelling had been performed in these tests. In this paper, an open-source experimental dataset is presented, and the dynamics of a concrete spar-based floating concept withstanding the IEA 15-MW Reference Wind Turbine are investigated. An experiment on a 1:55 scale concrete-based spar (WindCrete) at IHCantabria's ocean basin was developed by means of the hardware-in-the-loop technique under the COREWIND EU-H2020 project. The available data consist of the hydrodynamic characterizations and seakeeping tests with a total of 57 available datasets. The proper behaviour of the WindCrete platform and the designed mooring system is confirmed by the maximum motion values and accelerations below the established acceptance criteria defined. Moreover, this test program identifies the importance of the wind loads over the dynamic performance of the concept.

1. Introduction

The world energy demand is continuously increasing due to the increase in population, the development of emerging countries and the constant electrification of our economy. Society is increasingly aware of the impact of fossil fuels, which are considered responsible for greenhouse gas emissions and climate change. Therefore, many countries have either consolidated or are developing policies to favour the generation of energy through clean and low-carbon technologies. Currently, wind energy is the most important source of renewable electricity in the European Union (Eurostat, 2023). During the last five-year period, one out of five new wind installations in Europe has been offshore (Costanzo et al., 2023). The development of offshore wind energy technology has resulted in cost reductions that make such a technology economically competitive. Thus, offshore wind resources have become more reliable, and greater economies of scale with larger wind farms and larger turbines with taller towers reaching more suitable wind fields are possible. Capacity factors for new onshore wind farms are estimated at 30–35%, while for new offshore wind farms, this figure ranges between 42% and 55% (Costanzo et al., 2023).

On March 30th, 2023, the European Parliament and the Council reached a provisional agreement to raise the binding renewable energy target from the current 32% to at least 42.5% by 2030 to double the existing share of renewable energy in the EU at the end of 2019. The recent deal, which currently will add up to 111 GW of offshore wind capacity by 2030, will increase government commitments across Europe, and the EU goal of climate neutrality will require an increase of over 400 GW by 2050 (Cecchinato et al., 2021). Industrializing floating offshore wind will allow us to unlock 60% of Europe's offshore wind resources in areas with a water depth beyond 60 m, notably in the Mediterranean and Atlantic Oceans. Floating offshore wind will see significant cost reductions, decreasing by 65% from 2020 to 64 €/MWh by 2030 and converging the LCOE of bottom-fixed offshore wind by 2040 (Fraile et al., 2021).

The design of floating wind structures is currently one of the most complex engineering challenges since it is strongly dependent on highly nonlinear and coupled dynamics, such as the hydrodynamic actions on the floater and the aerodynamic response of the turbine (Somoano et al.,

* Corresponding author.
E-mail address: guancher@unican.es (R. Guanche).

https://doi.org/10.1016/j.oceaneng.2024.118612
Received 25 April 2024; Received in revised form 7 June 2024; Accepted 26 June 2024
Available online 29 June 2024

Mass properties w/o a turbine	
Mass [kg]	4.012e+07
Centre of Mass (CM) Height [m]	-98.50
Ixx [kg·m^2] from the CM	1.554e+11
Iyy [kg·m^2] from the CM	1.554e+11
Izz [kg·m^2] from the CM	1.915e+09
Mass properties with a turbine	
Mass [kg]	4.114e+07
Centre of Mass (CM) Height [m]	-92.76
Ixx [kg·m^2] from the CM	2.089e+11
Iyy [kg·m^2] from the CM	2.089e+11
Izz [kg·m^2] from the CM	1.992e+09
Hydrostatic properties	
Displacement [m^3]	4.054e+04
Centre of Buoyancy Height [m]	-77.29
C_{33} [N/m]	1.3746e+06
C_{44} [N·m/rad] from [0;0;0]	-3.1463e+10
C_{55} [N·m/rad] from [0;0;0]	-3.1463e+10
A_{33} [kg] from the CM	1.727e+06
A_{55} [kg·m^2] from the CM	8.964e+10
T_3 [s]	35
T_5 [s]	41

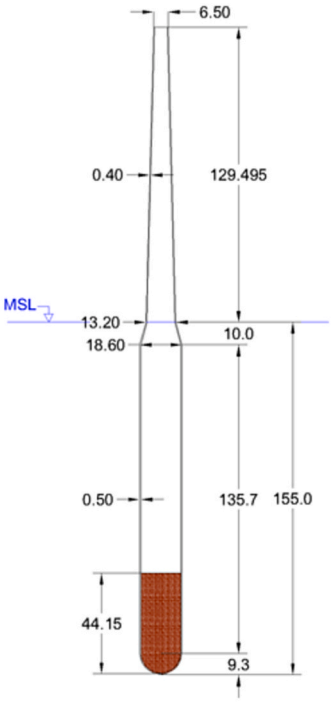

Fig. 1. WindCrete properties and sketch with values in metres (Mahfouz et al., 2020).

Table 1
Physical properties of the mooring system at full scale.

Line #		Chain bar diameter [mm]	Equivalent diameter [mm]	Line length [m]	Dry linear weight [kg/m]	Axial stiffness [kN]	Steel Grade
1	Main Line	111	199.8	700	245.19	10.52e5	R4
	Delta Lines	111	199.8	50	245.19	10.52e5	R3
2	Main Line	100	180	750	199	8.54e5	R3S
	Delta Lines	111	199.8	50	245.19	10.52e5	R3
3	Main Line	100	180	750	199	8.54e5	R3S
	Delta Lines	111	199.8	50	245.19	10.52e5	R3

Table 2
Anchor and fairlead locations of the mooring system at full scale.

Line #	Anchor Coordinates [m]			Fairlead coordinates [m]		
	X	Y	Z	X	Y	Z
1	−743.34	0	−200	−4.65	8.05	−90
				−4.65	−8.05	−90
2	396.33	−686.47	−200	−4.65	−8.05	−90
				9.3	0	−90
3	396.33	686.47	−200	−4.65	8.05	−90
				9.3	0	−90

2021a). To guarantee that a new concept can operate properly during its useful life and not jeopardize operational and structural integrity due to environmental actions, it is highly recommended to conduct thorough laboratory testing campaigns (Otter et al., 2022). Further experiments may be conducted in real environment with larger scales as the one conducted in the Gulf of Maine for the concrete base buoy VolturnUS in a 1:8 scale (Viselli et al., 2015). This experimental set-up has to deal with actual wind turbines and relevant environmental conditions.

At the laboratory scale, the difficulty in conducting floating offshore wind testing lies in the Reynolds number, which is not scaled properly at a reduced scale when adopting Froude scaling laws. The Froude scale is usually adopted when analysing the dynamic responses of floating offshore structures in ocean basin testing to reproduce gravity-influenced phenomena (Chakrabarti, 1998). Although the deviated reproduction of viscous forces is negligible in water, it has a significant influence on the aerodynamic response of a turbine (Muller et al., 2014). This incompatibility between the Froude and Reynolds numbers is a fundamental barrier when coupled hydrodynamic and aerodynamic actions need to be reproduced at the laboratory scale. This may be overcome by real-time hybrid modelling, which can be implemented to perform scale physical testing of the hydrodynamic problem (Chabaud et al., 2013). The other remaining problem, the aerodynamic problem, is simulated numerically in full scale in real time with the hardware-in-the-loop technique, while the aerodynamic forces are imposed in real time at the laboratory scale during the tests.

Azcona et al. described the implementation of this method based on the use of a ducted fan located at the model tower top in the place of the rotor (Azcona et al., 2014). The rpm of the fan can be adjusted to produce a variable force that represents the total wind thrust by the rotor. Thus, a computer simulation of the full-scale rotor is performed in synchronicity with the test. The platform motions (displacements and velocities) captured by the acquisition system are inputted in real time to provide the desired thrust to be introduced by the fan. However, this system cannot match the effect of gyroscopic momentum. Sauder et al. presented a detailed description of a system of tensioned cables with winches that can apply an aerodynamic thrust force and all aerodynamic load components of importance to the physical model (Sauder et al., 2016). This system consists of a minimal set of six actuators with pulleys fixed alongside the ocean basin and connected with thin lines to a square frame that is mounted at the nacelle location. Therefore, the numerical

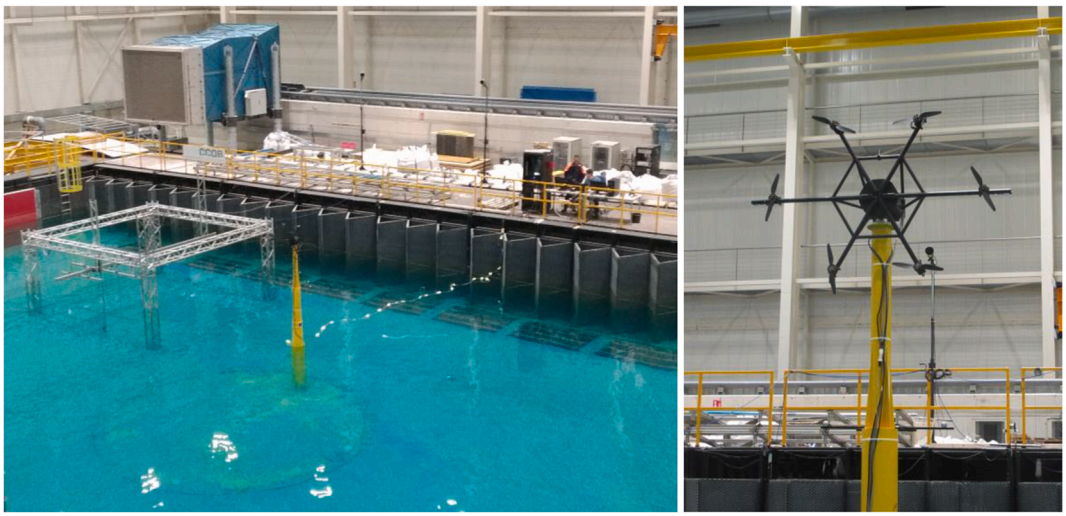

Fig. 2. CCOB facility (left) and IHCantabria multi-fan system (right).

Table 3
CCOB facility and IHCantabria multi-fan characteristics.

Length	30 m
Width	44 m
Max. Water depth	3.5 m (Central pit of 6 m diameter with 8 m extra depth).
Wave generation	Multidirectional long- and short-crested waves. Regular waves (3 m depth): up to H = 1.1 m (T = 3 s). Irregular waves (3 m depth): up to H_{m0} = 0.6 m (T_p = 3 s). periods T_p = 0.5–20 s (h = 0.2–3.7 m).
Wind generation	IHCantabria multi-fan constituted by an array of six fans operated independently and mounted at the tower top of the mockup.

The water depth used in the experiment was set to 3.0 m, which would imply a 165 m depth site. Then, the mooring system will be a truncated design, as presented in the following section.

substructure receives the kinematic data of the physical substructure as an input and returns the six components of the aerodynamic load vector to be applied on the top frame. Nevertheless, this set of winches must be placed in a specific auxiliary structure, increasing the complexity of the basin test setup. Moreover, the presence of tensioned cables that are always connected to the structure may cause undesired perturbations that affect the resonance response, altering the motions of moored floating structures (Gueydon et al., 2018).

Battistella et al. Meseguer and Guanche reproduced the most important aerodynamic loads by using a multi-fan system as the actuator at the hub height of the physical model (Battistella et al., 2018; Battistella et al., 2019; Meseguer and Guanche, 2019). The authors implemented a software in the loop in which the relative wind speed by the rotor is inputted into an unsteady blade element momentum (BEM) model as a function of the upscaled position of the platform that is

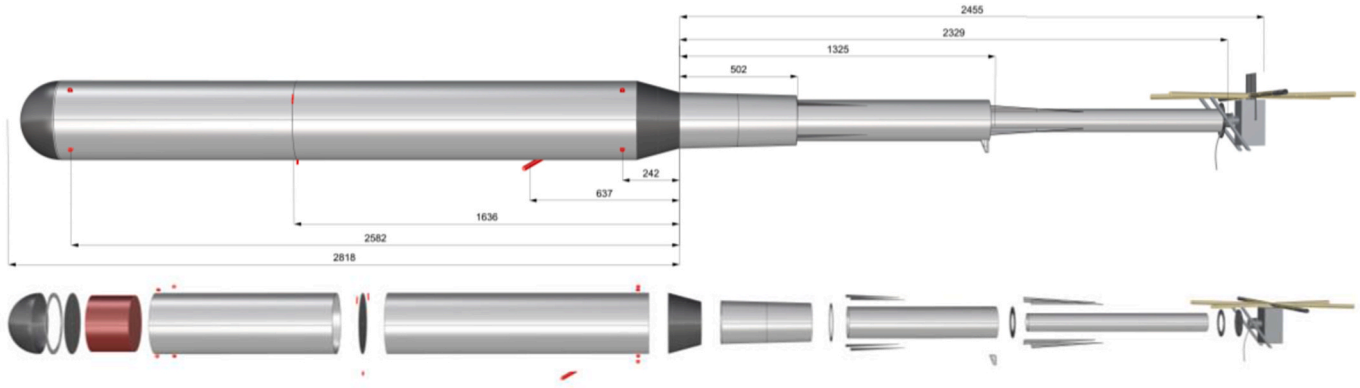

Fig. 3. Schematic (with values in millimetres) and breakdown of the *WindCrete* designed model.

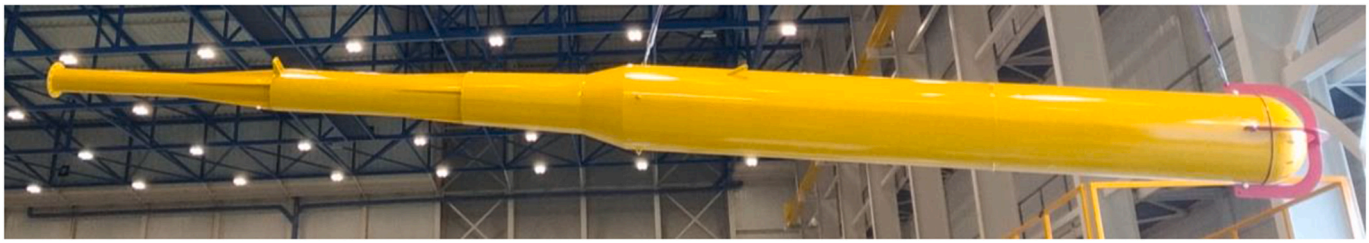

Fig. 4. WindCrete manufactured prototype hung by lugs at the FIHAC facility.

Table 4
Theoretical versus *as-built* mass, CoG position and inertia at the model scale.

	Mass [kg]	CoGx [m]	CoGy [m]	CoGz [m]	Ixx [kg·m^2]	Iyy [kg·m^2]	Izz [kg·m^2]
Target	241.242	−0.003	0	−1.687	404.950	404.950	3.861
Measured	241.639	−0.001	0	−1.695	409.312	406.768	3.986
Deviation	0.397	0.002	0	−0.009	4.362	1.818	0.125
Rel. Deviation [%]	0.16			0.51	1.08	0.45	3.23

Table 5
Physical properties of the mooring system at the model scale.

Line #		Chain bar diameter [mm]	Equivalent diameter [mm]	Line length [m]	Dry linear weight [kg/m]	Axial stiffness [kN]
1	Main Line	2.02	3.63	12.727	0.079	6.169
	Delta Lines	2.02	3.63	0.909	0.079	6.169
2	Main Line	1.82	3.27	13.636	0.064	5.008
	Delta Lines	2.02	3.63	0.909	0.079	6.169
3	Main Line	1.82	3.27	13.636	0.064	5.008
	Delta Lines	2.02	3.63	0.909	0.079	6.169

instantly provided by the high-resolution motion tracking system (i.e., *Qualysis)*. The aerodynamic loads numerically obtained from the BEM are applied downscaled with a system of up to six fans controlled individually by electro-servomotors. This system can be used to reproduce the wind turbine rotor thrust, out-of-plane rotor moments and aerodynamic and gyroscopic loads (Pires et al., 2020).

Spar concepts achieve hydrostatic pitch and roll stability through a low centre of mass far from the centre of buoyancy. There are some very recent studies related to the dynamic responses of spar wind turbines. For instance, Wang et al. numerically investigated the extreme loads that a spar platform supporting the DTU 10-MW reference wind turbine, experienced due to its pitch motion (Wang et al., 2023). However, few experimental research efforts on spar wind turbines can be found in the literature since this type of floater requires a deep wave basin because of its large draft. Nielsen et al. conducted model scale experiments for the Hywind concept for floating offshore wind turbines using a geometrically adjusted rotor with two DC motors for control of the rotational speed of the rotor and for the blade pitch angle based on estimates of the relative velocity between the physically incoming wind and the turbine (Nielsen et al., 2006). The DeepCwind consortium conducted a model test campaign of the OC3-Hywind spar designed to support a geometrically Froude-scaled model of the NREL 5-MW reference turbine (Goupee et al., 2014). To counteract the reduced aerodynamic forces on the turbine during testing, the physical wind speeds were increased to ensure appropriately scaled thrust forces, which is a key forcing component of wind on offshore wind systems. Ruzzo et al. studied the hydrodynamics of a Froude-scaled model of the UMaine-Hywind spar buoy, which differed from that of the OC3-Hywind only in the mooring system, in a field site off the beach of southern Italy (Ruzzo et al., 2016). The NREL 5-MW reference wind turbine was considered to be in the parked position, and it is represented by a lumped mass at the top.

The INNWIND project tested the Triple Spar floater, which is a hybrid between a spar buoy and a semi-submersible tri-floater, with a Froude-scaled model of the DTU 10-MW reference turbine with low-Reynolds aerofoils redesigned to deliver the target thrust with only a minor adjustment to the operational blade pitch angle (Bredmose et al., 2017). Hallak et al. analysed the hydrodynamic behaviour of the WIND-bos spar floating offshore wind turbine, whose hull is composed of two main bodies interconnected by means of three vertical steel legs, designed to accommodate the DTU 10-MW reference wind turbine (Hallak et al., 2022).

Moreover, the large draft of spar wind turbines usually limits their use to water depths higher than 200 m. If reproduced correctly, mooring lines would force the scale of the model to be too small, larger than 1:100 (Luo and Baudic, 2003), to correctly capture the hydrodynamic behaviour of the floater. It is then common practice to reproduce the mooring system of a structure with a truncated version of the properly scaled system. Thus, reasonable depths and footprints of the anchors can be achieved, and the influence of the mooring loads on the structure can be simultaneously reproduced. The truncation procedure is a well-established model scale testing method in the oil and gas industry (Fan et al., 2012). The truncated mooring system must satisfy some characteristics with respect to the full-scale system. Furthermore, the total horizontal restoring force must be correctly reproduced, the quasi-static coupling between the vessel responses must be modelled, and a representative level of damping and single line tension must be applied (Stansberg et al., 2001), with the latter being implemented in at least a quasi-static case (Molins et al., 2015). This approach, however, has the disadvantage of underestimating the peak forces in the cables, especially during survival load cases (Stansberg et al., 2004). A partial

Table 7
Anchor and connector locations of the truncated dynamic cable.

Truncated anchor coordinates [m]			Connector coordinates [m]		
X	Y	Z	X	Y	Z
6.966	0	−3.000	0.205	0	−0.664

Table 8
Physical properties of the dynamic cable at the model scale.

Line length [m]	Wet linear weight [kg/m]	Bending stiffness [N·m^2]
8.276	0.0146	4.3×10^{-5}

Table 6
Anchor and fairlead locations of the truncated mooring system.

Line #	Anchor Coordinates [m]			Truncated anchor coordinates [m]			Fairlead coordinates [m]		
	X	Y	Z	X	Y	Z	X	Y	Z
1	−13.515	0	−3.636	−8.846	0	−3.000	−0.085	0.146	−1.636
							−0.085	−0.146	−1.636
2	7.206	−12.481	−3.636	4.728	−8.207	−3.000	−0.085	−0.146	−1.636
							0.169	0	−1.636
3	7.206	12.481	−3.636	4.728	8.207	−3.000	−0.085	0.146	−1.636
							0.169	0	−1.636

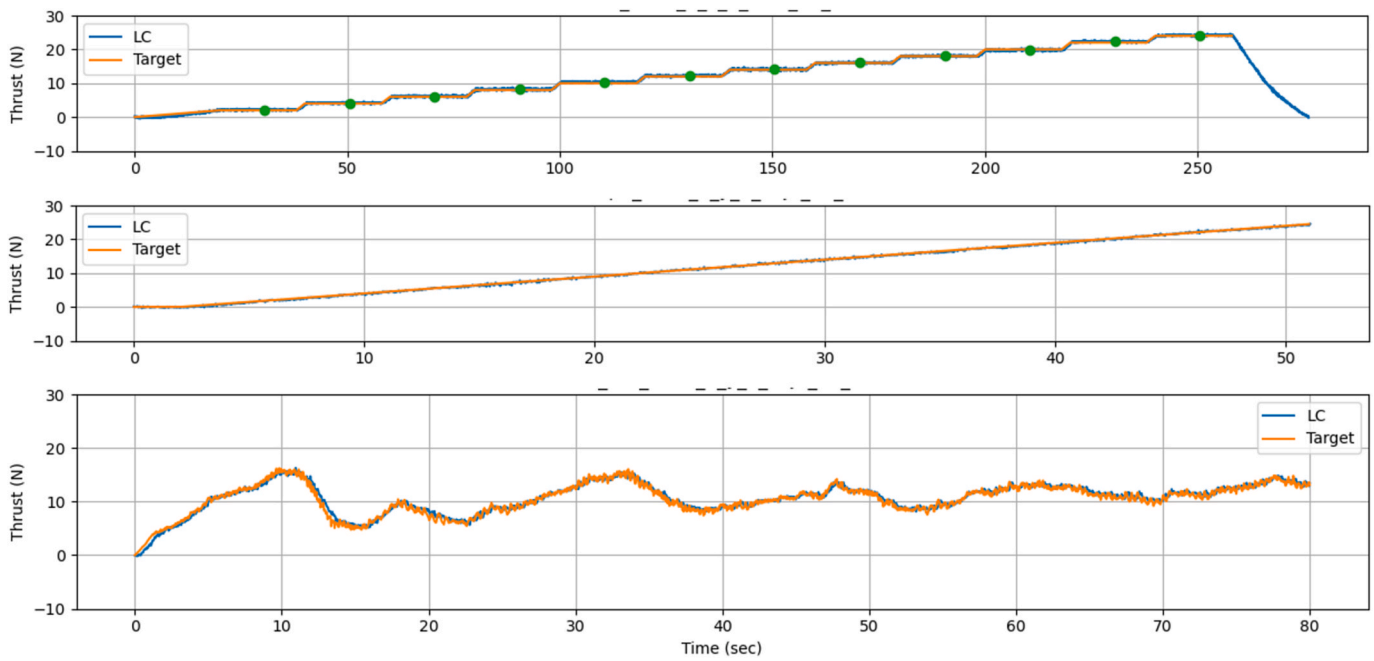

Fig. 5. Calibration of the IHCantabria multi-fan to step wind (top), ramp wind (centre) and rated wind (10.5 m/s) with the extreme turbulence model (ETM) (bottom).

Table 9
Placement of wave gauges in an array.

Id	X distance [m]	Y distance [m]
1–2	0.16	0
1–3	0.23	0
1–4	0.53	0
1–5	0.74	0
1–6	1.00	0
1–7	1.37	0
1–8	2.46	0
1–9	−0.534	−0.388
1–10	−0.534	0.388
1–11	0.204	−0.628
1–12	0.204	0.628

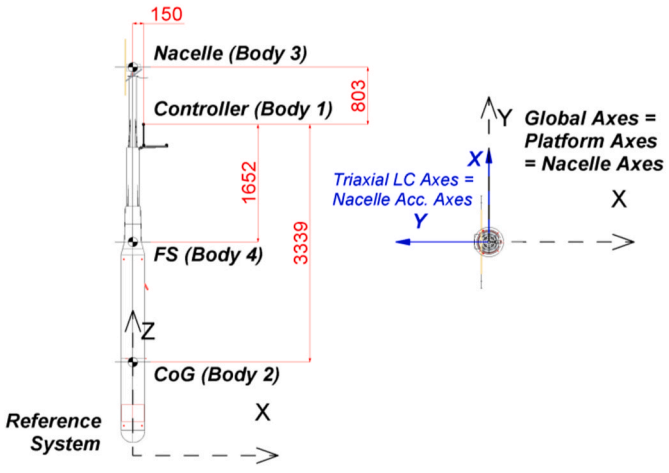

Fig. 6. Qualisys (with values in millimetres) and instrumentation reference systems (in contrast to the reference system used for the results).

solution to this issue is to use the real scaled mooring lines in the upper section, close to the fairleads, where dynamic loads are more important (Argyros et al., 2011).

Zhang et al. presented an optimization method to design a moored floating production storage and offloading (FPSO) system that works at a water depth of 320 m to a truncated water depth of 80 m (Zhang et al., 2012). They used an improved nondominated sorting genetic algorithm (INSGA-II) to match both the motion responses of the floater and the physical properties of the mooring system considering mainly the static characteristics. The same authors proposed the baton pattern-simulated annealing algorithm for hybrid discrete variables to optimize the static response of a single catenary and the whole catenary system static response in one direction to truncate a turret mooring FPSO from 304 m to 76 m water depth (Zhang et al., 2014). Molins et al. proposed an optimization method using the global search algorithm in MATLAB to design a truncated catenary mooring system that emulates the real mooring system of the monolithic concrete spar platform WindCrete for a 5-MW wind turbine (Molins et al., 2015). The optimization process was performed to adjust the quasi-static behaviour of the scaled mooring system, and a constant force on the nacelle was used to simulate the wind load.

To the knowledge of the authors, there is no publication in the literature regarding experimental test campaigns executed on a spar wind turbine by means of real-time hybrid modelling. Moreover, in the current experimental work, the concrete-based WindCrete concept supports the IEA 15-MW reference wind turbine (Gaertner et al., 2020), while the mooring system is truncated in the lower sections. The main goal is the generation of an open experimental database to be used as a benchmark of numerical models to leverage current and future investigations in the floating wind industry, as well as to deepen into the dynamics of the concrete spar-based floating offshore wind concept.

This paper is organized as follows. In Section 1, the state-of-the-art method is summarized to prove the novelty of the present work. In Section 2, the prototype configuration is presented. In Section 3, the model of the system is provided, and the experimental layout is defined after detailing the flume characteristics. In Section 4, the results of the experimental tests are presented. In Section 5, the obtained results are analysed, and any observations are discussed. Finally, in Section 6, the

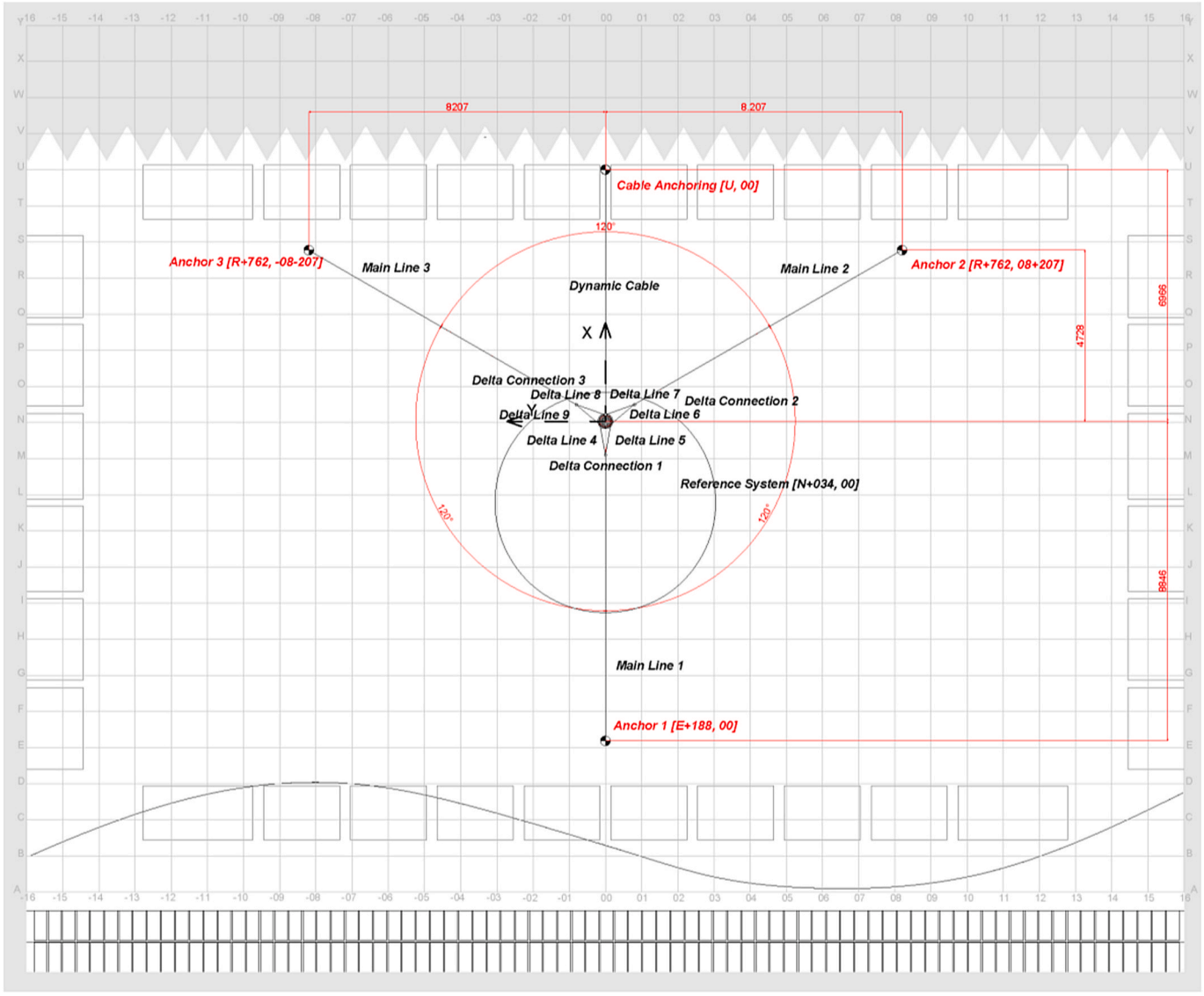

Fig. 7. Plan view of the experimental layout (with values in millimetres).

Table 10
Summary of the hydrodynamic characterization tests.

Test		Mooring	Configuration	DOF
01–03	*Decay tests*	Free floating	WC1	Heave, Roll, Pitch
04–09		Moored	WC2	Surge, Sway, Heave, Roll, Pitch, Yaw
10–11				Surge, Pitch below rated wind
12–13				Surge, Pitch with rated wind
14–15				Surge, Pitch above rated wind
16–17	*Static Offset tests*	Moored	WC2	Positive Surge, Negative Surge

Table 11
Wind test matrix (all values are presented at full scale).

Test	Wind [m/s]	Thrust [tonnes]	Duration
18	10.5	236.34	1 h
19	10.5 ETM	170.62	1 h
20–22	9, 10.5, 18 NTM	173.92, 192.06, 94.18	1 h

conclusions of the described study are summarized.

2. Description of the prototype

WindCrete is a monolithic concrete spar platform that includes both the tower and the floater in a unique concrete member developed at UPC (Campos et al., 2016). Compared to an equivalent steel platform, the concrete-based WindCrete concept offers a significant cost reduction not only in the construction phase but also during its operation lifetime due to the maintenance savings. Because of the monolithic nature of the platform, there are no joints between the tower and the floater. Hence, the fatigue resistance is increased since weak points are reduced. The structural design accounts for longitudinal active reinforcement to avoid tractions at any point during the lifespan of the platform by giving an initial compression state.

The WindCrete prototype used for the experimental setup is designed to withstand the IEA 15-MW reference wind turbine for the Gran Canaria site, which was developed during the COREWIND project. The main properties of the design are summarized in Fig. 1. The centre of mass height refers to the free surface. Note that the presented hydrostatic

Table 12
Seakeeping test matrix (all values are presented at full scale).

REGULAR WAVE TESTS				COMBINED REGULAR WAVE AND STEADY RATED WIND TESTS					
Test	H [m]	T [s]	Duration	Test	H [m]	T [s]	Wind [m/s]	Thrust [tonnes]	Duration
23–28	2.75	7.5, 9, 11, 14, 17, 20	200 waves	46–51	2.75	7.5, 9, 11, 14, 17, 20	10.5	234.36, 231.73, 227.04, 218.26, 215.72, 216.02	200 waves
29–34	5.11	7.5, 9, 11, 14, 17, 20	200 waves						
IRREGULAR WAVE TESTS					COMBINED IRREGULAR WAVE AND WIND TESTS					
Test	Hs [m]	Tp [s]	JS	Duration	Test	Hs [m]	Tp [s]	JS	Wind [m/s]	Thrust [tonnes]	Duration
35–37	2.75	9, 11, 14	$\gamma = 3.3$	3 h	52	2.75	9	$\gamma = 3.3$	10.5 ETM	174.26	3 h
38–39	5.11	9, 11	$\gamma = 1.2$	3 h	53–55	5.11	9	$\gamma = 1.2$	9, 10.5, 18 NTM	176.71, 194.76, 92.23	3 h
40–41	2.75	9	$\gamma = 3.3, s = 6, 12$	3 h	56–57	2.75	9	$\gamma = 3.3, s = 6, 12$	10.5 ETM	175.29, 175.21	3 h
42–43	5.11	11	$\gamma = 1.2, s = 6, 12$	3 h							
WHITE NOISE WAVE TESTS											
Test	Hs [m]	T1 [s]	T2 [s]	Duration							
44–45	2.75, 5.11	7.5	22	3 h							

properties contain only the influence of the buoyancy.

On Gran Canaria Island, gentle environmental loads combined with a water depth of 200 m can be used to develop chain mooring lines. The mooring system is composed of three catenary lines equipped with a crowfoot system known as a delta connection, which helps to increase the yaw stiffness. Three types of chains are used. Table 1 summarizes the physical properties of each chain, while Table 2 gives the anchor and fairlead coordinates.

The dynamic cable is designed as a lazy wave configuration in which the buoyant section decouples the dynamic motions of the platform from the touchdown point fixed on the subsea end. The cabling system is configured equidistant between Mooring Lines 2 and 3. The exit angle azimuth of the J-tube is 30° outwards from vertical down. The connection point is at a depth of 36.5 m below sea level and 2 m away from the edge of the structure. A high-voltage cable JDR 66 kV with CW002 size was selected for the modelling cables. The nominal bend stiffness is 22.2 kN m^2, and the nominal weight in seawater is 45.4 kg/m with buoyancy modules of 527.5 kg of net buoyancy force in the buoyant section.

3. Experimental set-up

Considering the dimensions and generation capabilities of the Cantabria Coastal and Ocean Basin (CCOB), it was concluded that 1:55 was the most suitable test scale to carry out the physical experiments on the WindCrete platform.

3.1. Basin characteristics

The wave-wind coupled tests were conducted at the CCOB facility managed by IHCantabria (Spain), as shown in Fig. 2. The right-hand side of the figure shows the IHCantabria multi-fan system used to reproduce the aerodynamic forces at the hub height of the experimental setup. To implement the hardware-in-the-loop technique, apart from the structure geometry, the rotor aerodynamic characteristics and the wind turbine controller, the numerical modules also considered the turbine movements which contribute to the calculation of the relative wind speed seen by the rotor. In subsequent real-time instants, the platform model positions and velocities provided by an optical tracking system were provided to the numerical code, after being upscaled to prototype scale to avoid the incompatibility between Reynolds and Froude scaling laws. During the same loop, the aerodynamic forces got from an unsteady BEM model were scaled back to model scale to operate the IHCantabria multi-fan system at the hub height of the mockup.

The main characteristics and generation capabilities of the multi-directional wave basin as well as those of the IHCantabria multi-fan device are described in Table 3.

3.2. Physical model characteristics

Both concrete mass of the structure and solid aggregate ballast have been simulated with steel in the WindCrete mockup. In fact, most of the platform physical model was engineered and manufactured in steel, except for the lower hemisphere of the spar which was made of acrylonitrile butadiene styrene (ABS) by means of a 3D printer. The junction of this element with the submerged spar was waterproof. Fig. 3 includes geometrical and mass properties of the different designed elements that made up the physical model, following Froude's scaling laws of similitude (RP-C205, D. N. V. G. L., 2017). The lower hemisphere made of ABS was protected with a removable steel strut (painted in red) to avoid any structural damage before entering the wave basin (Fig. 4).

A dimensional and weight distribution control was carried out in the dry characterization to ensure the quality of the manufactured prototype, fulfilling the tolerances demanded. Table 4 reports the comparison between the targeted mass properties and those obtained during the quality control tests of the prototype. The centre of gravity in Z refers to the free surface.

The laboratory mooring system was built using conventional steel chains that reproduce the linear weight. Assuming the chain is infinitely rigid, the axial stiffness of the full mooring system is replicated by means of calibrated springs located at the anchors (Somoano et al., 2022; Somoano et al., 2024). The targeted physical properties of the chains and calibrated springs to be used at a laboratory scale of 1:55 are summarized in Table 5. The length and weight of the springs are included in the properties of the main lines, and the provided stiffness is given in the axial stiffness column.

Because of the limits of the basin dimensions, the main lines of the mooring system were truncated in both the water depth and footprint size (Table 6). The aim of the truncation method was designing a truncated system set-up which replicated the static offset curves computed for the real lines. The methodology applied for the numerical modelling of the single mooring line static truncation was based on nonlinear catenary equations and evolutionary optimization algorithms. The constrained Genetic Algorithm, implemented in MATLAB, could find

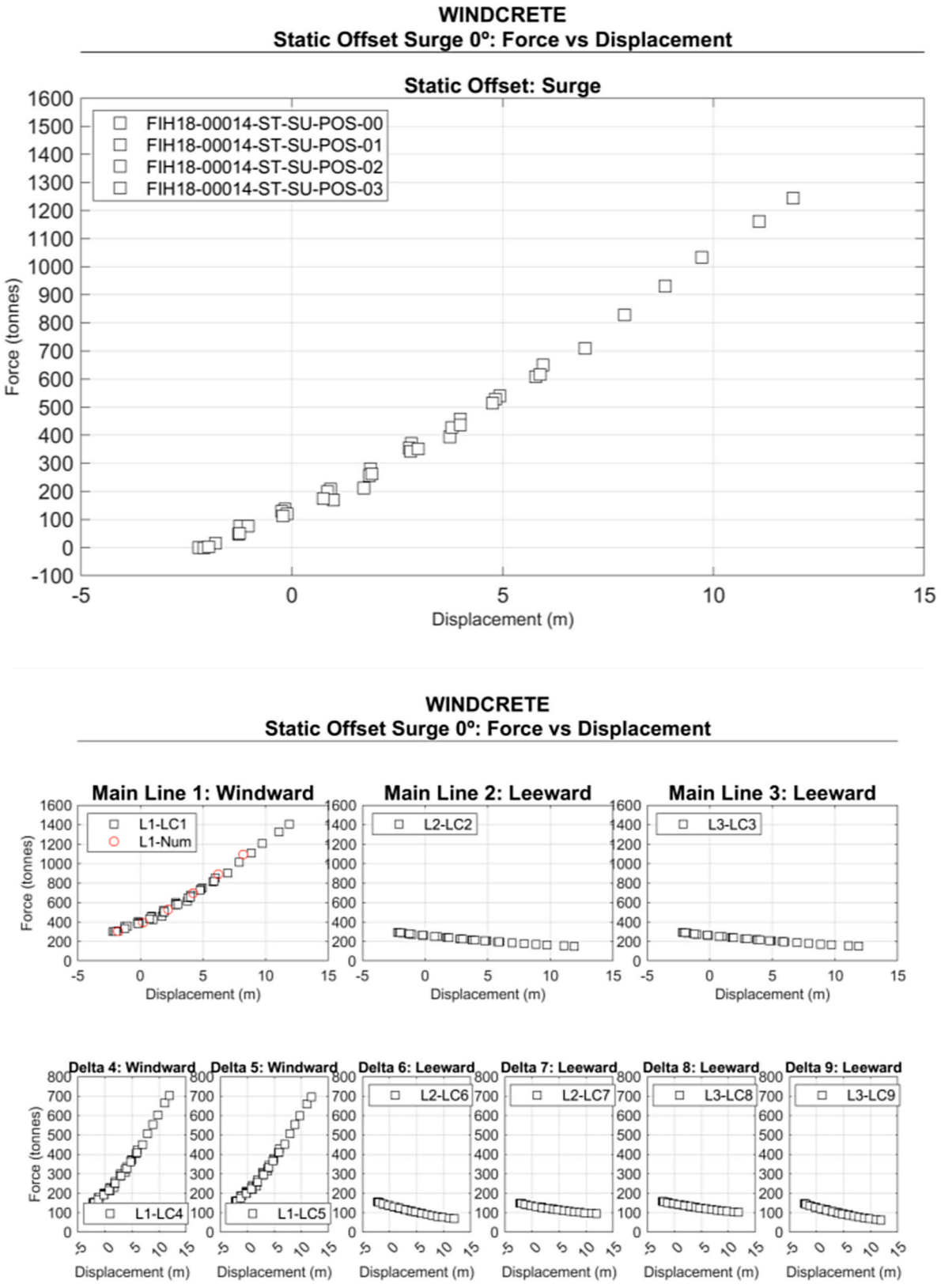

Fig. 8. Applied force (up) and mooring forces (down) versus platform displacements in positive surge.

several local minimums of the objective function which was the mean of the four NMSE (Normalised Mean Square Error) of the horizontal and vertical forces in the line along the horizontal and vertical axis. Previous experience in line truncation was used to create an appropriate initial population, and the Genetic Algorithm was hybridized with a pattern search algorithm to improve the solutions found (Goldberg, 1989; Audet and Dennis, 2002). The truncated mooring system was designed to be as simple as possible to reduce uncertainties and simplify numerical model validation.

The laboratory dynamic cable was also truncated because of the

Table 13
Natural periods (T) and nondimensional damping coefficients (D) obtained during the decay tests.

	Surge		Sway		Heave		Roll		Pitch		Yaw	
	T (s)	D (%)	T (s)	D (%)	T (s)	D (%)	T (s)	D (%)	T (s)	D (%)	T (s)	D (%)
Free floating					35.41	0.69	41.42	0.90	41.10	0.79		
Moored	79.23	8.01	82.94	6.02	34.73	1.60	41.30	0.64	41.02	0.89	16.18	6.37
Moored below rated wind	66.48	15.20							48.74	19.83		
Moored with rated wind	66.63	14.30							44.78	9.53		
Moored above rated wind	75.55	10.51							42.30	6.23		

limits of the basin dimensions, as reported in Table 7.

The truncated dynamic cable was built using an appropriate elastic material that reproduces both the linear weight and the bending stiffness. To correctly replicate the dynamic performance of the power cable, Somoano et al. built a three-point bending flexural tester and developed a methodology for the reproduction of bending stiffness using elastic materials (Somoano et al., 2022). From the generated catalogue of these elastic materials, the targeted physical properties of the elastic string model to be used at a laboratory scale of 1:55 are summarized in Table 8. In the buoyant section, there are 20 buoyancy modules with a net buoyancy force of 3.1 g equally spaced at 91 mm.

The turbine aerodynamic loads are defined and generated by means of a hardware-in-the-loop (HIL) layout developed at IHCantabria (Pat. ES 2 632 187 B1). The setup contains the IHCantabria multi-fan system (right side of Fig. 2), which is a device constituted by an array of six fans that operated independently to generate rotor aerodynamics with high fidelity. The array is mounted at the tower top of the prototype to maintain the correspondence between the position of the resultant of the forces generated by the multi-fan itself and the centre of the turbine rotor. The capability to reproduce aerodynamic loads with high accuracy is guaranteed by an adequate calibration procedure (Urban and Guanche, 2019). The result of such practice allows us to limit the error of the generated thrust at less than 3% of the target value. Fig. 5 shows the comparison between the generated thrust measured by a tri-axial load cell (blue line) and the target value pursued by the aforementioned numerical module (orange line) in the calibration of the IHCantabria multi-fan to three different winds. Note that at the end of the time series on top (step wind), the generated thrust in the tri-axial load cell at the nacelle is still being recorded once the target value is not imposed anymore.

3.3. Basin instrumentation

Before introducing the physical model in the CCOB facility, each selected sea state was calibrated in the absence of FOWT to prevent disturbances upon the basin free surface measurements. During the wave calibration stage, two arrays of free surface gauges (AWP-24 from Akamina Technologies) were used. The incident and reflected waves in both arrays were calculated by applying the Mansard and Funke methodology (Mansard and Funke, 1980). The first set of sensors, referred to as the calibration array, was placed in the basin starting from the origin of the reference system (X and Y coordinates of the centre of the platform in quiet conditions) and was removed after the wave calibration phase. The second array, referred to as the control array, was located parallel to the calibration array and was maintained in the same position during the whole test campaign as a reference to verify the validity of the generated sea-state conditions during the seakeeping tests. Table 9 shows the distances between the twelve wave gauges of the same array with respect to the first array, with the X coordinate being the predominant wave direction.

The Qualisys Tracking Motion system was used to evaluate the hydrodynamic performance of WindCrete. The movements in 6 DOF were measured in the centre of gravity and the nacelle of the wind turbine as well as in the geometric centre of the intersection between the floating platform and the mean water level (the origin of the reference system was used to obtain the results). Fig. 6 on the left presents the heights of the different bodies in which the movements are recorded.

A tri-axial load cell (K6D40 from ME-Systeme) and an accelerometer (Model 4030) were installed at the nacelle to measure the forces and moments in 6 DOF together with the RNA accelerations in the X, Y and Z directions. The sign convention used during the test program is shown in Fig. 6. The loads on the mooring system were measured using a set of axial force transducers (Tecsis F2808) located at the six fairleads and the three delta connections. Fig. 7 presents the positions of the axial load cells in the experimental set-up, where the number refers to the load cell (LC) identification number.

4. Description of the experimental tests

The experimental tests, after introducing the physical model in the CCOB facility, were divided into hydrodynamic characterization tests consisting of decay tests, static offset tests and seakeeping tests to evaluate the performance of *WindCrete* under different wind-wave conditions.

4.1. Hydrodynamic characterization tests

The characterization tests (as shown in Table 10) are essential to validate that the model behaviour reflects that of the designed full-scale prototype for both the platform and mooring system. To determine the metacentric height GM, tilt tests are usually conducted for both the pitch and roll rotations in free-floating conditions by applying a weight at several distances such that each eccentricity with respect to the platform applies a different moment. However, reliable inclination tests cannot be executed in a monolithic spar platform, and a hydrostatic analysis with AQWA software was carried out instead.

Decay tests were performed to obtain the natural periods and the nondimensional damping coefficients (Journée and Massie, 2000). These tests were carried out in free-floating (Configuration WC1), in heave/roll/pitch and in moored conditions (Configuration WC2) in all 6 DOFs, as well as in surge/pitch with rated, below-rated and above-rated wind speeds. When executed in free floating conditions (WC1), clump weights were added at the fairleads to replicate the vertical tensions of the delta mooring lines.

The aim of the static offset tests is to validate the stiffness of the mooring system. These tests can be conducted to evaluate the stiffness of the mooring for positive and negative surge displacements in Configuration WC2 by progressively displacing the platform while measuring the force needed to apply the displacement.

4.2. Wind tests

After the characterization tests, a set of wind tests with rated, below-rated and above-rated wind speeds were performed. During the execution of the wind tests, the time series of the motions, mooring line loads, accelerations and thrust are recorded. In addition, the rotor thrust calculated by the hardware-in-the-loop is analysed. Table 11 summarizes the parameters of the wind tests included in the campaign: constant rated wind (10.5 m/s); rated wind with the extreme turbulence model (ETM); and rated, below-rated (9 m/s) and above-rated (18 m/s) winds

Table 14
Static condition of movements and mooring system loads under wind action.

Wind [m/s]	Motions at CoG - Mean Static Position						Main and Delta Lines - Mean Mooring Loads							
	X [m]	Y [m]	Z [m]	Roll [deg]	Pitch [deg]	Yaw [deg]	ML1 [tonnes]	ML2 [tonnes]	ML3 [tonnes]	DL4 [tonnes]	DL5 [tonnes]	DL6 [tonnes]	DL7 [tonnes]	DL8 [tonnes]	DL9 [tonnes]
–	−1.93	1.28	−1.66	0.23	0.51	1.14	295.60	280.26	281.64	147.98	153.04	149.06	142.94	154.08	137.11
10.5 Steady	1.46	0.94	−1.57	0.50	4.77	1.02	470.51	230.40	244.76	235.65	236.41	138.63	100.70	119.31	132.02
10.5 ETM	0.92	1.05	−1.61	0.44	3.67	1.07	422.33	238.60	249.59	210.17	214.39	139.23	110.85	126.70	132.25
9 NTM	1.15	1.08	−1.64	0.46	4.03	1.06	436.76	233.99	245.49	217.24	221.24	137.98	107.46	123.46	131.57
10.5 NTM	0.91	1.09	−1.66	0.44	3.70	1.04	422.48	237.77	248.31	210.36	213.99	138.91	110.39	126.42	131.53
18 NTM	−0.20	1.17	−1.68	0.34	2.29	1.06	362.70	253.59	260.11	180.97	184.69	142.28	123.04	137.59	132.17

with the normal turbulence model (NTM). All wind tests are conducted with the WC2 configuration at 0° and a depth of 165 m.

4.3. Seakeeping tests

Regular and irregular waves with and without wind, as well as white noise tests, were executed. The selection of the environmental parameters is based on the Gran Canaria location (Vigara et al., 2019), and all of them are given at the prototype scale. The range of regular wave periods (T) was from 7.5 to 20 s for two different wave heights (H) of 2.75 m and 5.11 m and for a constant rated wind speed (10.5 m/s). With respect to the irregular wave, peak periods (Tp) were between 9 and 14 s for two different significant wave heights (Hs) of 2.75 m and 5.11 m and for the four different winds: rated wind with the extreme turbulence model (ETM); and rated, below rated (9 m/s) and above rated (18 m/s) winds with the normal turbulence model (NTM). The JONSWAP wave spectrum is defined by the peak enhancement factor (γ) and the spreading (s) in the case of short-crested waves. Furthermore, white noise tests were carried out to build the platform RAOs from 7.5 to 22 s for two different significant wave heights of 2.75 m and 5.11 m. Without including neither a set of operational sea states simulating currents (1.06 m/s) nor a set of installation tests because these tests are not discussed in the present paper, a total of 57 tests were carried out. All the seakeeping tests (Table 12) are conducted with the configuration WC2 at 0° and a depth of 165 m.

5. Results and discussion

5.1. Hydrodynamic characterization tests

As previously mentioned, spar-based structures are complex structures based on metacentric characterizations. The inclination tests usually performed to obtain the GM by applying a weight such that its eccentricity with respect to the platform applies a moment, could not be conducted in this case. Therefore, an analytical method that can be used to measure the as-built GM has been proposed. The actual draft of 156.65 m, instead of 155 m, is implemented in AQWA software because of the negative deviation in the diameter and the positive deviation in the weight when manufactured, and the hydrostatic analysis results in a GM of 14.89 m is obtained. This analytical approach may introduce uncertainty in the result. Nevertheless, if we had carried out the tilt tests, since the weight cannot be placed far away from the Z axis, the mass required to achieve an inclination of the platform would have introduced much more uncertainty.

Fig. 8 shows the results of four repetitions of static offset tests in a positive surge. The first position is the static position once the platform is moored, with X lower than −1.75 m because the origin of the reference system was defined for a previous nonoptimized mooring system. On the left, the force needed to displace the platform is plotted against the applied displacement. The axial forces measured in the main mooring lines and in the delta mooring lines are plotted on the top right and on the bottom right, respectively, as a function of the same platform displacements.

The natural periods and the nondimensional damping coefficients of the specific DOF resulting from the decay tests are presented in Table 13. The results shown are the mean values of the five times that each decay test was repeated to ensure the statistical representativeness. As expected, higher nondimensional damping coefficients are presented in the surge, sway and yaw. The mooring system decreases the natural periods in the heave, roll and pitch. In the presence of wind, the natural periods decrease in the surge but increase in the pitch. In the case of the surge, the thrust forces increase the stiffness of the mooring system and therefore lower the natural periods. It is important to note that in both DOFs, the differences with and without wind are higher below-rated wind speeds than with rated wind, which in turn is higher than above-rated wind, as expected. However, the aerodynamic damping effect is

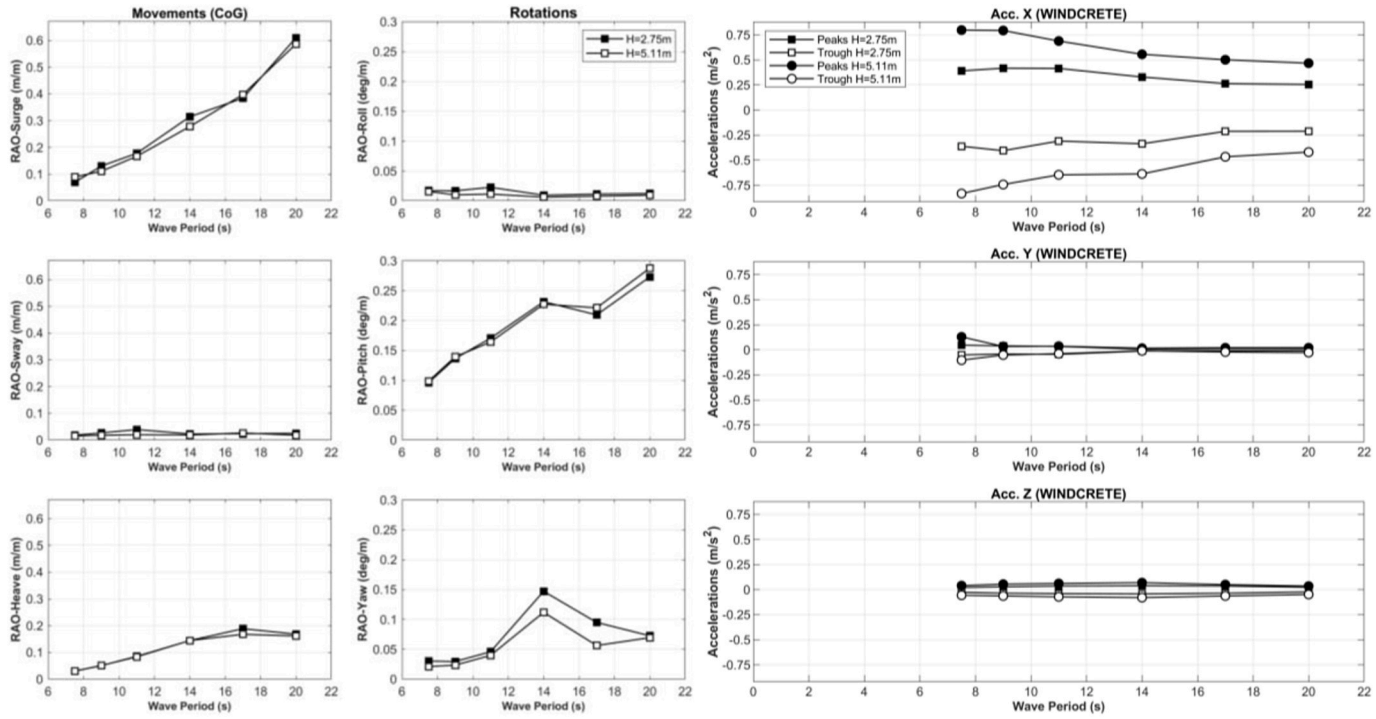

Fig. 9. RAOs of motions at the centre of gravity (left) and positive/negative mean values of nacelle accelerations (right) under regular wave action.

seen by the slight change in the periods (Hmedi et al., 2022).

5.2. Wind tests

Table 14 presents the mean static position of the CoG, as well as the mean mooring system loads, to evaluate the influence of different wind conditions on the WindCrete. The initial platform positions and mooring system loads without wind action are also included as a reference. As mentioned above, the static position of CoG has a Z of −1.65 m due to the actual draft. On the other hand, X is lower than −1.75 m for a positive pitch because the inertial reference is at the fairlead's depth for a previous nonoptimized mooring system. As expected, Mooring Line 1 is the most loaded without any wind action, and the sum of the loads of a couple of delta lines is always higher than that of the main line at which they are connected.

Based on Table 11, the minimum mean thrust was applied for above-rated wind (18 m/s) with the normal turbulence model (NTM), increasing for rated wind (10.5 m/s) with the extreme turbulence model (ETM), below-rated wind (9 m/s) with the NTM, and rated wind with the NTM to obtain the maximum value for steady-rated wind. As the mean thrust is increased, WindCrete is displaced in the surge, and a pitch angle is induced. The maximum offset and tilt angle are 3.39 m and 4.26 deg, respectively, obtained with steady rated wind. With respect to the mean mooring loads, the larger the mean thrust is, the larger the tension in Mooring Line 1. The tension in Main Line 1 with steady rated wind is increased by 59.17% compared to the nonwind condition.

5.3. Seakeeping tests

The current section provides motions and accelerations of WindCrete, as well as mooring system loads, for different wind-sea states in the case of application of singular and coupled environmental conditions with the aim of understanding the seakeeping behaviour and the dynamics of the floating wind turbine concept.

5.3.1. Regular wave tests

Figs. 9 and 10 present the rigid body motion, accelerations and loads obtained from regular wave tests without wind (Table 12). This set of tests provided the data necessary to obtain the WindCrete experimental response amplitude operators (RAOs), which are illustrated on the left of Fig. 9. These RAOs are obtained as the mean value of the distance between the peaks and troughs over the incident wave height and indicate the natural periods under regular wave conditions. The movement amplifications in the surge, heave and pitch are below 0.7 m/m, 0.2 m/m and 0.3 deg/m, respectively. In this configuration, a coupling between the yaw and pitch motion can be observed in the pitch RAO with a peak at 14 s period, but the maximum pitch RAO of almost 0.3 deg/m appears for a 20 s period. Moreover, it is important to note that in terms of the movements, the 6 DOFs show minor differences between the RAO computed based on H = 2.75 m or H = 5.11 m. The maximum differences can be seen on the yaw DOF, which might be due to the nonlinear behaviour of the delta line (30% less excitation in the Yaw-RAO calculated with the highest wave height). Finally, it can be said that the dynamic performance of the FOWT shows a very limited nonlinearity up to a wave height of 5.11 m, since both RAOs in the rest of the DOFs are almost equal.

Regarding nacelle accelerations, the mean peak/trough value of the time series are represented as a function of the wave period on the right of Fig. 9. Even for the highest wave slope (H = 5.11 m, T = 7.5 s), these values are always below ±1 m/s^2 and hence further down than the acceleration limits of the IEA 15-MW nacelle (Table 15). Despite showing a linear performance in terms of the displacements, the structure shows significant differences between the means of the peak and trough values computed with H = 2.75 m and those obtained from the H = 5.11 m waves for accelerations at the tower top. Tower top accelerations are mainly governed by the pitch. Therefore, a very limited nonlinear pitch performance will lead to highly nonlinear dynamics in the tower top acceleration performance due to the amplification given by the tower height.

With respect to the mooring tensions, the mean peak/trough value of the time series, together with the static loading as a reference, are plotted against the wave period in Fig. 10. The behaviour of the mooring system is directly related to the horizontal displacement in the surge, reaching the highest values of the mean peak/trough in Main Line 1 at

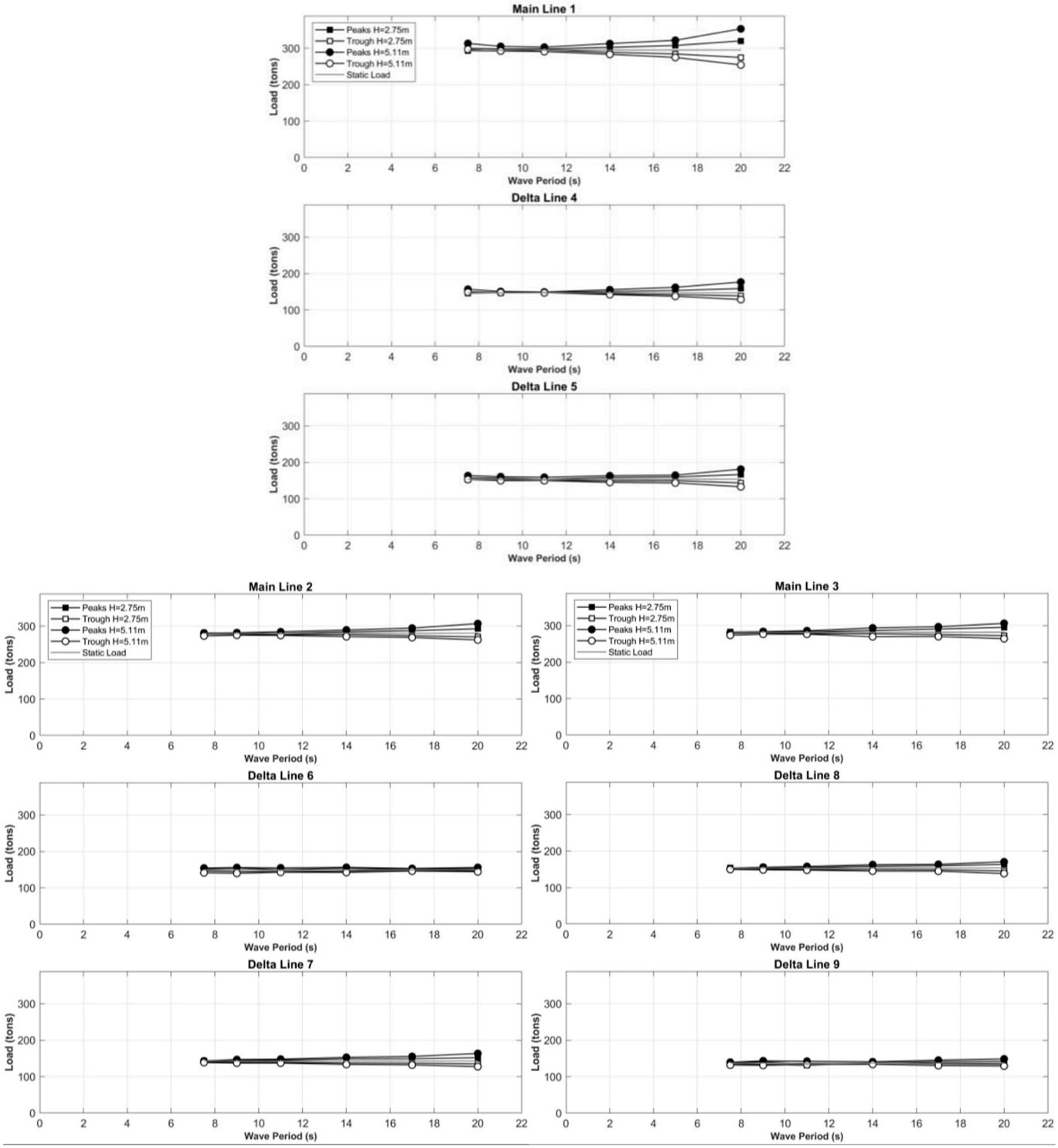

Fig. 10. Mean peak/trough values of the mooring loads in seaward (top) and leeward lines (bottom) under regular wave actions.

the seaward direction for a wave height of 5.11 m and a period of 20 s. In addition, Delta Lines 7 and 8 at the inner leeward support most of the mean loading amplitude of the main lines to which they are connected.

5.3.2. *Combined regular wave and steady-rated wind tests*

Figs. 11 and 12 present the rigid body motion, accelerations and loads obtained from regular wave tests with a steady rated wind (Table 12). The RAOs have been obtained analogously to the previous section.

It is important to note that the heave and surge motions show a similar pattern as in the case without wind, with movement amplifications below 0.7 m/m and 0.2 m/m, respectively. However, in this configuration, the pitch and yaw motions show significant differences, and the maximum pitch RAO of almost 0.3 deg/m appears for period T = 14 s at which the RAO in the yaw presents a resonant peak. That means that the yaw stiffness provided by the delta lines are enough to overcome the coupling motion between yaw and pitch. Regarding nacelle accelerations, the mean peak/trough value of the time series are

Table 15
Design of the WindCrete limits (angular motions, excursions and accelerations).

OPERATION		EXCURSION RESTRICTIONS (100 m)	
Yaw (10 min max)	<15°	**DoF/Limit typology**	**Limit**
Yaw (10 min std)	<3°	Horizontal offset (alarm limit) (mean during operation)	30 m
Pitch (max.)	[-7.5°, +7.5°]	Horizontal offset (WTG shutdown). Maximum during parked conditions	60 m
Pitch (10 min average)	[-4.0°, +4.0°]	**ACCELERATIONS LIMITS**	
Roll (max.)	[-3.5°, +3.5°]	Operation (acc. XY/acc. Z)	2.80 m/s^2 (0.28 g)
Pitch (10 min std)	<1°	Survival (acc. XY/acc. Z)	3.50 m/s^2 (0.35 g)
Roll (10 min std)	<1°		
IDLING CONDITION			
Pitch (10 min average)	[-5°, +5°]		
Pitch (10 min max)	[-10°, +10°]		
EMERGENCY STOP			
Max. pitch	[-15°, +15°]		

represented as a function of the wave period on the right of Fig. 11. The accelerations of the nacelle in the X-direction are highly dependent on the wave height of 2.75 m, being always below ±0.5 m/s^2 as under regular waves without wind.

With respect to the mooring tensions, the mean peak/trough value of the time series, together with the static loading without wind as a reference, are plotted against the wave period in Fig. 10. Under regular waves without wind, Delta Lines 7 and 8 at the inner leeward direction support most of the mean loading amplitude of the main lines to which they are connected, and the highest value of the mean peak is obtained in Main Line 1 at the seaward direction for a wave period of 20 s. However, in this case, the maximum tension reaches 557 tonnes because the steady rated wind action causes a mean offset of the platform. Wind loads are one order of magnitude larger than the drift forces from regular waves (Sarmiento et al., 2019). The mean offset may be observed when comparing the mean peak/trough to the static loading reference. Without wind (Fig. 10), static loading occurs between the mean peak and mean trough values for both seaward and leeward mooring lines. Conversely, with steady rated wind, static loading without wind is below the mean trough values for windward mooring lines and over mean peak values for leeward mooring lines. Wind loads also introduce important changes in the mooring dynamics since the oscillations between the maximum and minimum values of the mooring loads under an incident wave height of 2.75 m increase more than three times in the presence of steady rated wind.

5.3.3. *Irregular wave tests*

Figs. 13 and 14 show the mean/maximum/minimum values of the WindCrete movements at CoG, nacelle accelerations and mooring loads obtained from irregular wave tests without wind (tests numbering of the X axis follows Table 12). The highest amplitudes in the surge and heave displacements, as well as in the pitch rotations, are obtained for irregular waves with a significant height of 5.11 m (Fig. 13 on the left). In the surge and heave, the amplitudes are higher for the peak period of 9 s because of the larger wave slope, while in the pitch, the amplitudes are higher for the larger peak period of 11 s. As expected for both cases of significant heights, short-crested waves present lower amplitudes in the surge, heave and pitch but higher amplitudes in the sway, roll and yaw in comparison to long-crested waves. However, the highest amplitude in the yaw rotation is obtained for the long-crested wave with a significant height of 2.75 m and a peak period of 14 s, in agreement with the resonant peak obtained for the regular wave and the natural period measured in the moored decay tests in this DOF.

The highest nacelle accelerations in the X-direction are also obtained for irregular waves with a significant height of 5.11 m (Fig. 13 on the right). These values are always below ±2 m/s^2 and thus are beneath the

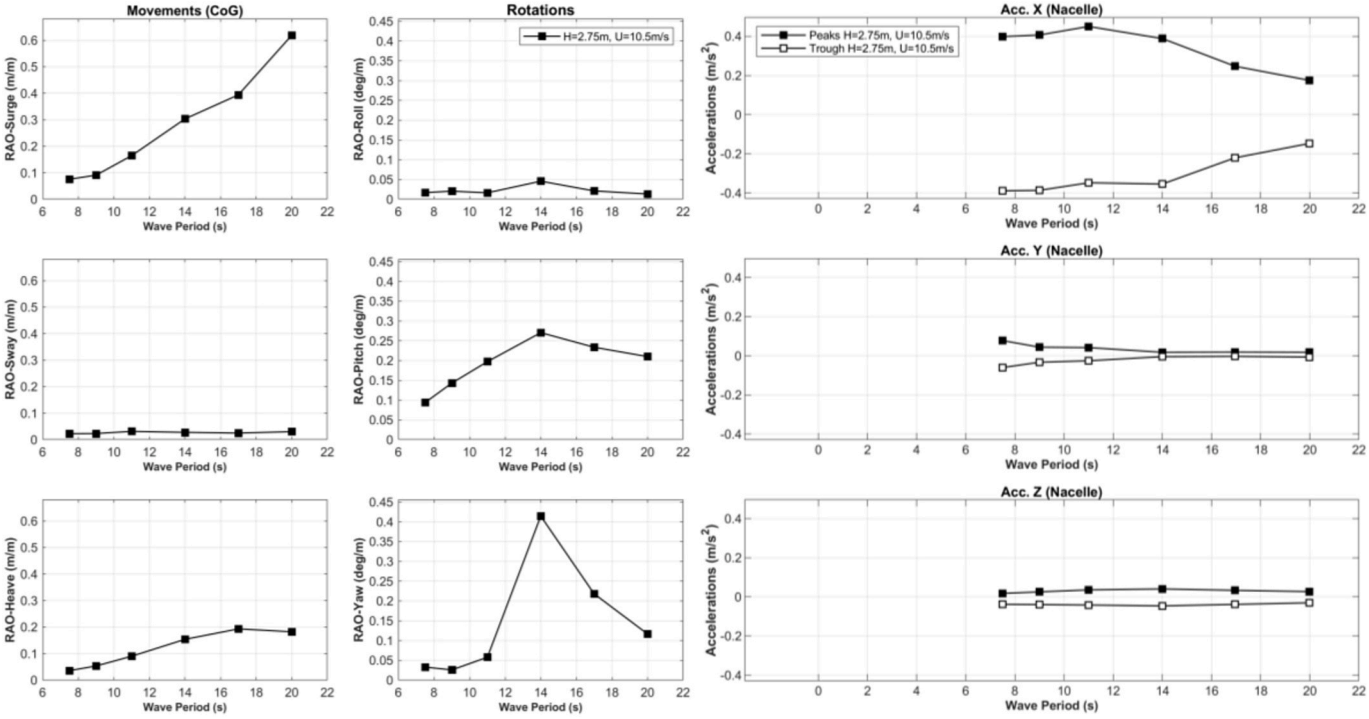

Fig. 11. RAOs of the motions at the centre of gravity (left) and positive/negative mean values of nacelle accelerations (right) under combined regular wave and steady rated wind actions.

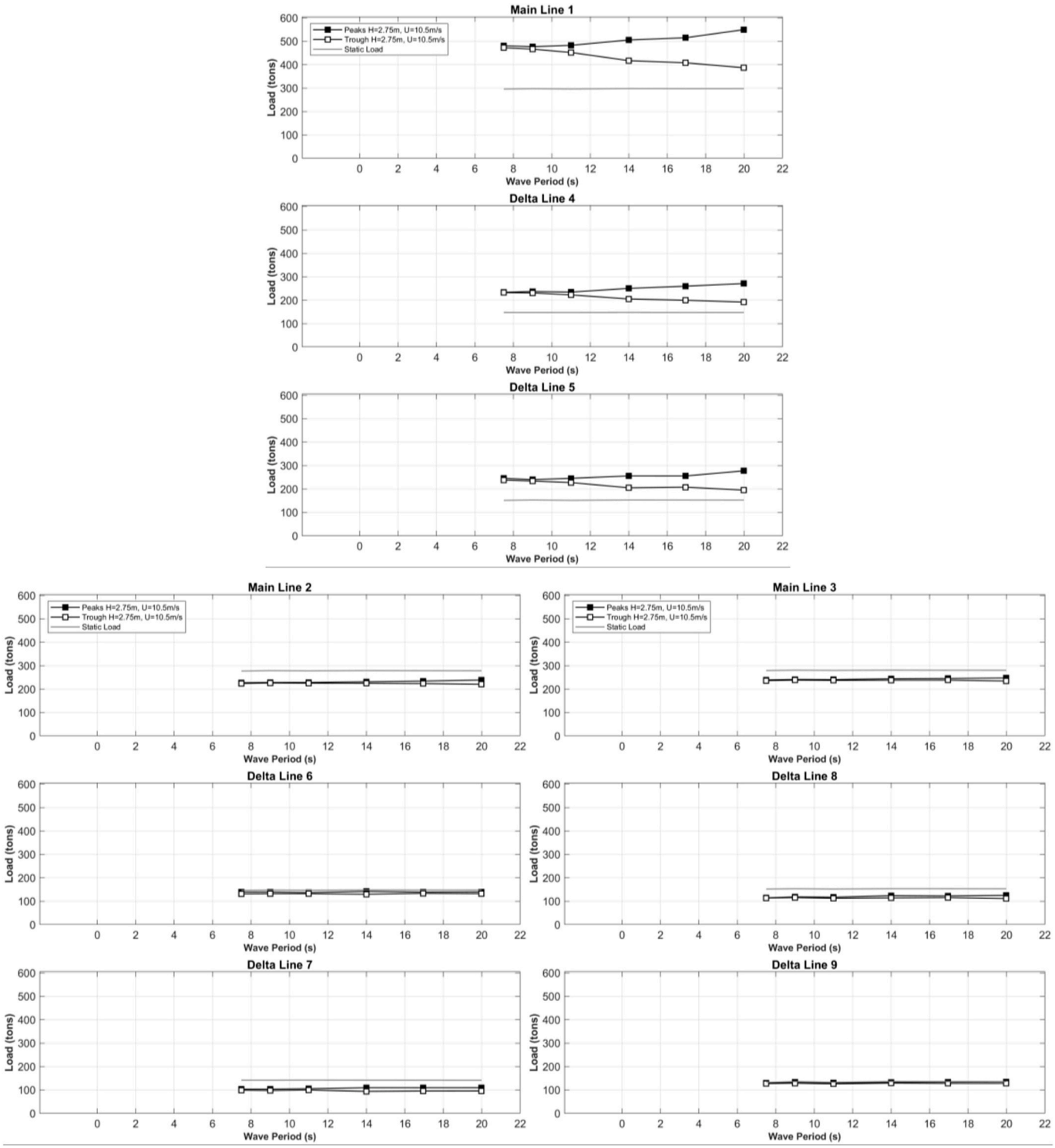

Fig. 12. Mean peak/trough values of the mooring loads in seaward (top) and leeward lines (bottom) under combined regular waves and steady rated wind actions.

acceleration limits of the IEA 15-MW nacelle (Table 15). As expected for both cases of significant heights, short-crested waves present lower nacelle accelerations in the X-direction but higher values in the Y-direction in comparison to long-crested waves. The behaviour of the mooring system (Fig. 14) is directly related to the horizontal displacement in the surge, reaching the maximum tensions in Main Line 1 at the seaward direction for long-crested waves with a significant height of 5.11 m.

5.3.4. Combined irregular wave and wind tests

Figs. 15 and 16 show the mean/maximum/minimum values of WindCrete movements at CoG, nacelle accelerations and mooring loads obtained from irregular wave tests with non-steady wind (tests numbering of the X axis follows Table 12). The higher the mean thrust is (based on Table 11), the larger the mean offset of the platform, and the higher the mean pitch induced, causing an elevation in the mean heave (Fig. 15 on the left). The highest amplitudes in the surge (3.79 m) and pitch (6.43 deg) are obtained for rated wind with the extreme turbulence

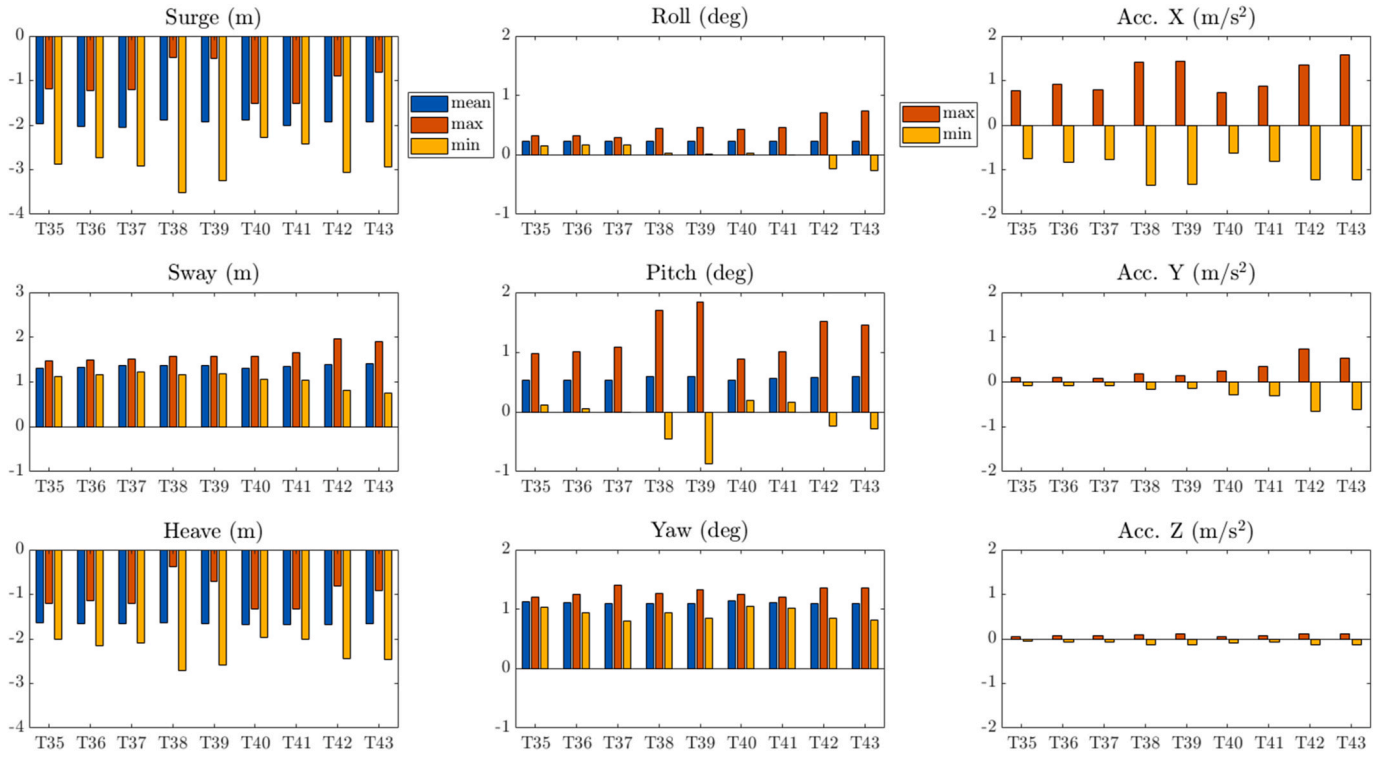

Fig. 13. Mean/maximum/minimum values of motions at the centre of gravity (left) and maximum/minimum values of nacelle accelerations (right) under irregular wave actions.

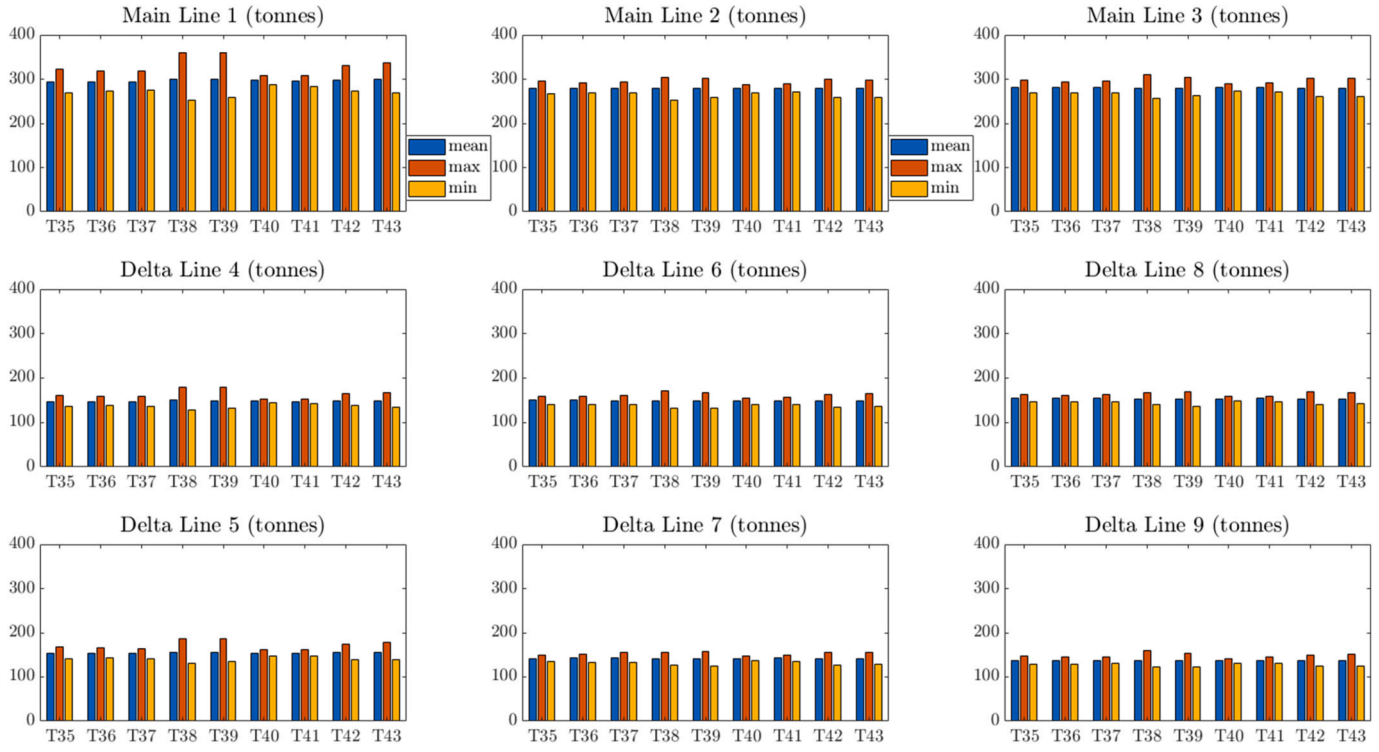

Fig. 14. Mean/maximum/minimum values of the mooring loads in the main (top) and delta lines (bottom) under irregular wave actions.

model. In the presence of wind, short-crested waves present similar values in the surge and sway in comparison to long-crested waves. However, the highest amplitudes in the heave displacements are caused by irregular waves with a significant height of 5.11 m. The heave displacements of the platform exhibit no dependence on the wind loads (Somoano et al., 2021b). The accelerations of the nacelle in the X-direction are also highly dependent on the wave height, obtaining the highest values for irregular waves with a significant height of 5.11 m (Fig. 15 on the right). These values are always below ± 2 m/s^2 and thus are beneath the acceleration limits of the IEA 15-MW nacelle (Table 15).

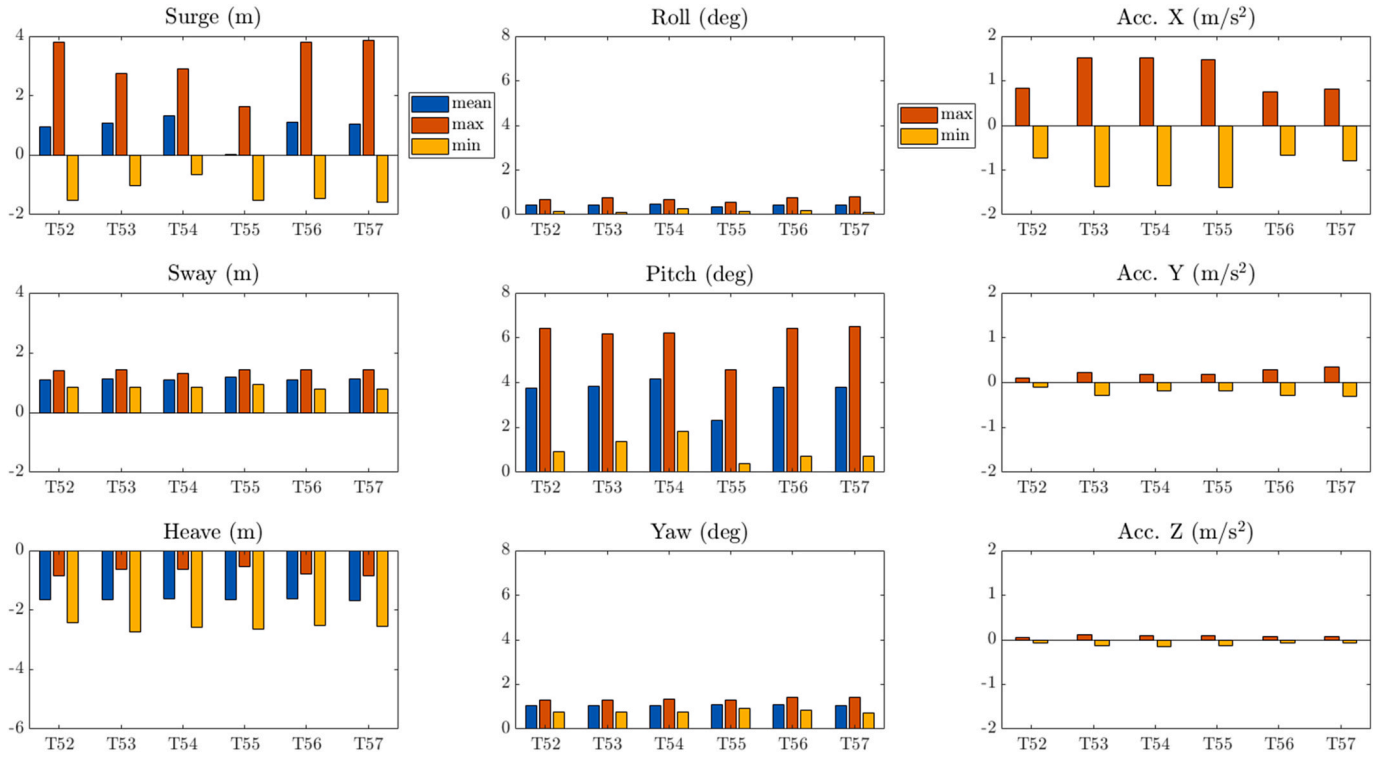

Fig. 15. Mean/maximum/minimum values of motions at the centre of gravity (left) and maximum/minimum values of nacelle accelerations (right) under combined irregular waves and wind actions.

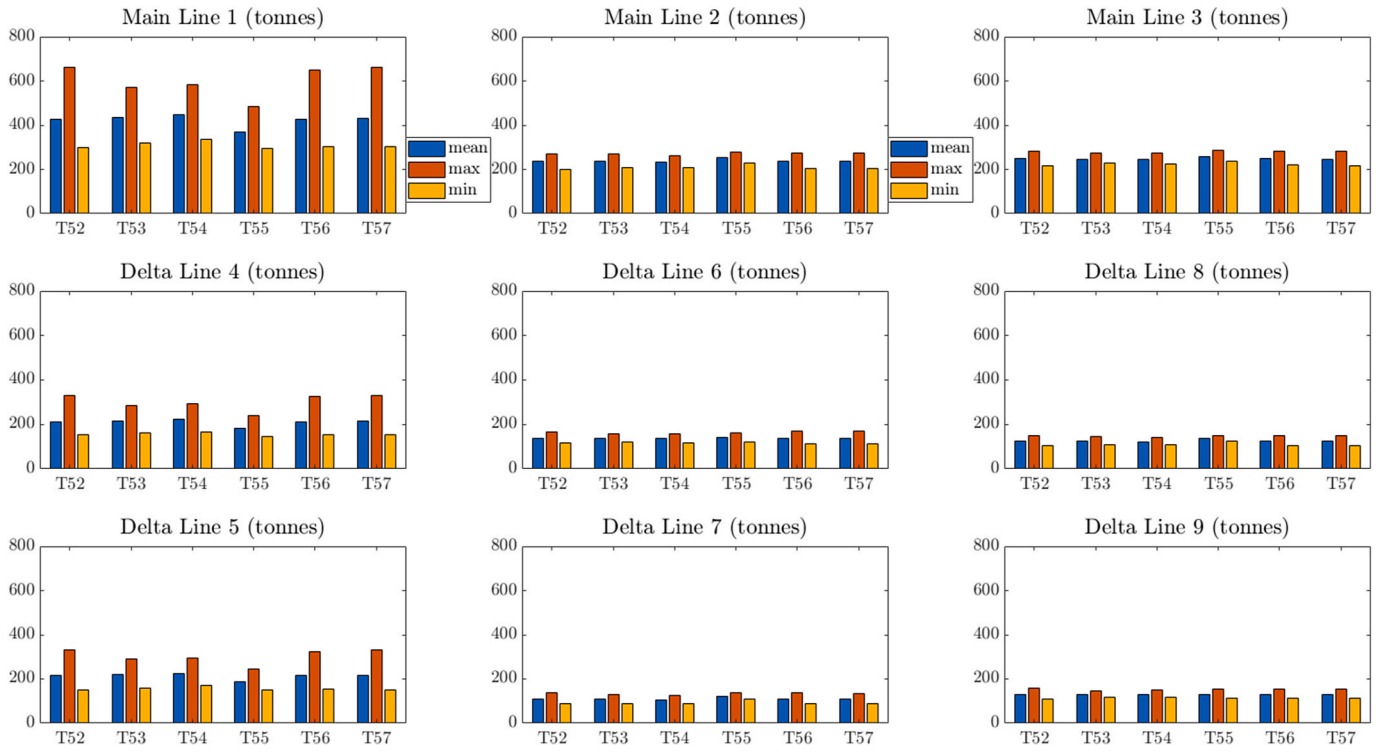

Fig. 16. Mean/maximum/minimum values of the mooring loads in main (top) and delta lines (bottom) under combined irregular wave and wind actions.

In addition, short-crested waves present lower nacelle accelerations in the X-direction but higher values in the Y-direction in comparison to long-crested waves with the same significant height and peak period.

The behaviour of the mooring system (Fig. 16) is directly related to the horizontal displacement in the surge. The higher the mean thrust is, the larger the mean offset of the platform, and the higher the mean tensions in the windward mooring lines (and the lower the mean tensions in the leeward mooring lines). Without wind, static loading (based on Table 11) is similar to the mean values of the mooring loads for both the seaward and leeward mooring lines (Fig. 14). Conversely, in the

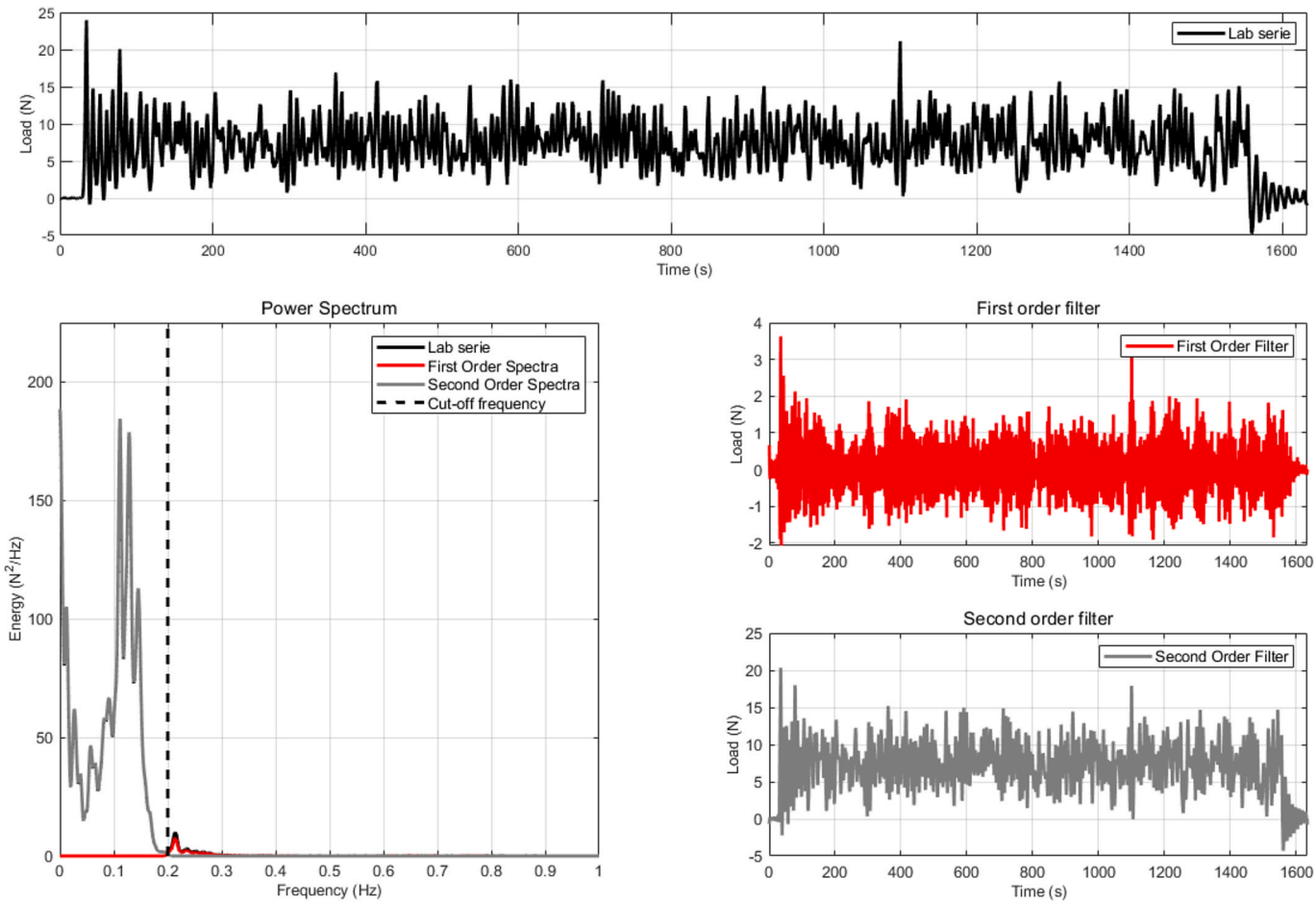

Fig. 17. Decomposition of the load time series in Main Line 1 into high and low frequencies for the most severe operational wind-sea state (Hs = 2.75 m, Tp = 9 s and γ = 3.3 with rated wind with ETM) at the laboratory scale.

presence of wind, the mean values of the windward mooring loads are over, while the mean values of the leeward mooring loads are below static loading without wind. The wind loads also introduce important changes in the mooring dynamics since the amplitudes between the maximum and minimum values of the mooring loads increase more than six times in the presence of turbulent wind. The highest amplitudes in the surge and the highest amplitudes in the mooring loads are obtained for rated wind with the extreme turbulence model. Therefore, the maximum tension in Main Line 1 at the windward direction equal to 663 tonnes is reached in the case of Hs = 2.75 m, Tp = 9 s and γ = 3.3 with rated wind with ETM.

For the most severe operational wind-sea state (Hs = 2.75 m, Tp = 9 s and γ = 3.3 with rated wind with ETM), Fig. 17 on the top presents the total load time series (black line) in Main Line 1 at the windward direction at the laboratory scale. On the bottom, the load time series has been decomposed into high (red line) and low frequencies (grey line), with a cut frequency of 0.2 Hz, as shown in the power spectrum. From Table 11, the rated wind with ETM introduces an extra mooring load offset of 126.73 tonnes, which is an increase of 42.87% in comparison to the nonwind condition. Moreover, from Fig. 8, the maximum dynamic load and a major part of the standard deviation of the mooring line forces are directly related to turbulent wind effects. At low frequencies, the surge motions of the platform are dominated by the wind conditions (Somoano et al., 2021b).

5.4. Acceptance criteria

FOWT design limit criteria for operation, idling and emergency stop conditions must ensure the good behaviour of the different subsystems. These limits are set to prevent damage to the different subsystems due to overexposure to large loads produced for excess pitching, large nacelle acceleration or large offsets. These limits are very difficult to establish and may involve different OEM criteria for the different subsystems that are not publicly shared.

Within the COREWIND project, these limits have been established for WindCrete as a reference value for design and verification purposes. As the IEA 15-MW Reference Wind Turbine was developed for research purposes, these limits are not specified, so the values presented in Table 15 should be considered as a starting reference point, and detailed load studies should be carried out to verify the reliability of the different FOWT subsystems. The values of Table 15 are based on COREWIND D1.2 (Vigara et al., 2019), but the pitch maximum values have been increased. The increase is justified because the structure can resist the increase in the loads.

As stated in the analysis of the experimental data, the WindCrete platform fulfils all the requirements of the design limits established in this section.

6. Conclusions

In this paper, the experimental setup, the experimental data and the analysis of the results performed on the WindCrete platform developed by UPC to withstand the IEA 15-MW Reference Wind Turbine at IHCantabria within the COREWIND project are presented.

The scale factor used for the experimental setup is 1:55 to maximize the platform geometry while maintaining a feasible representation of

the selected location, Gran Canaria. The WindCrete mock-up was built with steel except for the base hemisphere. The IEA 15-MW Wind Turbine was emulated using the multi-fan developed at IH Cantabria with hardware in the loop system to account for the platform motions to assess the actual thrust due to the relative wind by applying the BEM solution in real time, which makes the first available experimental spar platform that uses a hybrid approach.

The presented data are based on the experimental tests performed during September–October 2022, which consist of a total of 57 test conditions. The experimental tests consist of three setups: 1) hydrodynamic characterization (Test 01 - Test 17), wind tests (Test 18 – Test 22) and seakeeping tests (Test 23 – Test 57). The hydrodynamic characterization is performed with a free floating (WC1) and a moored configuration (WC2). The wind tests were performed to study the wind conditions at rated, below-rated and above-rated wind speeds to characterize the thrust force over the platform. The seakeeping tests performed are composed of regular wave tests, irregular wave tests, white noise wave tests, combined regular wave and steady rated wind tests and combined irregular wave and wind tests.

The fully coupled experimental tests can be used to characterize the response of the WindCrete platform in different conditions for operational at-rated, below-rated and above-rated wind conditions. Regular wave tests were used to obtain the RAOs of the platform showing amplification factors below unity, which are always a good indicator of platform seakeeping characterization. The seakeeping tests also confirm the proper behaviour of a spar platform with maximum motion values and accelerations below the established acceptance criteria defined for the WindCrete within the COREWIND project. For a spar platform, the coupling between pitch and yaw can lead to large non-linear motions exceeding the established limits due to the low damping in the yaw DOF. However, the designed mooring system shows a proper behaviour at these DOFs, presenting a slight excitation with motions lower than the limits. The analysis of the experimental results also confirms the large contribution of the wind low-frequency range excitation compared to the wave frequency excitation range. This is a clear breakthrough compared to platforms with lower power wind turbines, where the wave excitation contribution is relatively larger. This influence can be clearly seen in the windward mooring line tension energy spectra analysis.

In summary, this paper contributes to increasing the knowledge of spar platform seakeeping behaviour against dynamic wind and irregular waves by using a hybrid approach to characterize wind turbine loads. The data will help to validate hydro-servo-elastic models or high-fidelity models such as CFD for spar platforms, which can improve the still poor knowledge and representativity of hydrodynamic interaction between waves and platforms. Moreover, the use of hardware in the loop wind turbine setup is proven, and satisfactory performance is achieved to emulate the IEA 15-MW Reference Wind Turbine.

Nevertheless, the current experimental study is limited to hydrodynamic characterization, wind tests and seakeeping tests for different wind-sea states in the case of application of singular and coupled environmental conditions. A future work may discuss either the effect on mooring line tensions of adding current to the operational sea states simulated or the platform stability during installation and erection from horizontal to vertical position. On the other hand, and in order to verify the drawn conclusions, further experiments may be conducted in real environment where there is no limit on water depth and the concrete-based WindCrete concept may be tested at larger scales.

CRediT authorship contribution statement

M. Somoano: Writing – original draft, Formal analysis, Data curation. **P. Trubat:** Writing – original draft, Formal analysis, Data curation. **R. Guanche:** Writing – review & editing, Methodology, Funding acquisition, Conceptualization. **C. Molins:** Writing – review & editing, Funding acquisition, Conceptualization.

Declaration of competing interest

The authors declare that they have no known competing financial interests or personal relationships that could have appeared to influence the work reported in this paper.

Acknowledgements

This work is part of the COREWIND project, which has received funding from the European Unions Horizon 2020, Research and Innovation programme under Grant Agreement No. 815083. R. Guanche also acknowledges Grant RYC-2017-23260 funded by the Spanish Ministry of Science and Innovation, MCIN/AEI/10.13039/501100011033 by “ESF Investing in your future”.

References

Argyros, A., Langley, R.S., Ahilan, R.V., 2011. Simplifying Mooring Analysis for Deepwater Systems Using Truncation. Maui, IH, USA, s.N.
Audet, C., Dennis, J.E., 2002. Analysis of generalized pattern searches. SIAM J. Optim. 13 (3), 889–903.
Azcona, J., et al., 2014. Aerodynamic thrust modelling in wave tank tests of offshore floating wind turbines using a ducted fan. s.l. J. Phys. Conf., 012089
Battistella, T., Meseguer, A., Guanche, R., 2019. Real Time Hybrid Model Testing Including Complex Aerodynamic Loading for TRL+ project. Copenhagen (Denmark), s.N.
Battistella, T., Paradinas, D.D.L.D., Urbán, A.M., Garcia, R.G., 2018. High Fidelity Simulation of Multi-MW Rotor Aerodynamics by Using a Multifan. s.l., s.n.
Bredmose, H., et al., 2017. The Triple Spar campaign: model tests of a 10MW floating wind turbine with waves, wind and pitch control. Trondheim (Norway). Energy Proc. 58–76.
Campos, A., Molins, C., Gironella, X., Trubat, P., 2016. Spar concrete monolithic design for offshore wind turbines. In: Proceedings of the Institution of Civil Engineers - Maritime Engineering, 169, pp. 49–63, 2.
Cecchinato, M., Ramírez, L., Fraile, D., 2021. A 2030 Vision for European Offshore Wind Ports: Trends and Opportunities. s.l., WindEurope.
Chabaud, V., Steen, S., Skjetne, R., 2013. Real-time hybrid testing for marine structures: challenges and strategies. s.l. In: Proceedings of the International Conference on Offshore Mechanics and Arctic Engineering - OMAE.
Chakrabarti, S., 1998. Physical model testing of floating offshore structures. Houston (TX, USA). In: Proceedings of the Dynamic Positioning Conference.
Costanzo, G., Brindley, G., Cole, P., 2023. Wind Energy in Europe: 2022 Statistics and the Outlook for 2023-2027. s.l., WindEurope.
Eurostat, 2023. Shedding Light on Energy in the EU. s.l., European Union.
Fan, T., Qiao, D., Ou, J., 2012. Optimized Design of Equivalent Truncated Mooring System Based on Similarity of Static and Damping Characteristics. s.l., s.n, pp. 959–966.
Fraile, D., et al., 2021. Getting Fit for 55 and Set for 2050: Electrifying Europe with Wind Energy. s.l., WindEurope.
Gaertner, E., et al., 2020. IEA Wind TCP Task 37: Definition of the IEA 15-Megawatt Offshore Reference Wind Turbine. NREL, Golden (CO, US).
Goldberg, D.E., 1989. Genetic Algorithms in Search, Optimization & Machine Learning, s.l.. Addison-Wesley.
Goupee, A., et al., 2014. Experimental comparison of three floating wind turbine concepts. J. Offshore Mech. Arctic Eng. 136 (2), 020906.
Gueydon, S., Lindeboom, R., Van Kampen, W., De Ridder, E.-J., 2018. Comparison of Two Wind Turbine Loading Emulation Techniques Based on Tests of a TLP-FOWT in Combined Wind, Waves and Current. s.l., s.n.
Hallak, T., et al., 2022. Hydrodynamic analysis of the WIND-Bos spar floating offshore wind turbine. J. Mar. Sci. Eng. 10, 1824.
Hmedi, M., et al., 2022. Experimental analysis of CENTEC-TLP self-stable platform with a 10 MW turbine. J. Mar. Sci. Eng. 10, 1910.
Journée, J., Massie, W., 2000. Offshore Hydromechanics. TU Delft, Delft.
Luo, Y., Baudic, S., 2003. Predicting FPSO Responses Using Model Tests and Numerical Analysis. s.l., s.N, pp. 167–174.
Mahfouz, M.Y., et al., 2020. COREWIND D1.3: Public Design and FAST Models of the Two 15MW Floater-Turbine Concepts, s.l.: USTUTT, ESTEYCO, UPC, DTU.
Mansard, E., Funke, E., 1980. The measurement of incident and reflected spectra using a least squares method. Sidney (Australia). In: Proceedings of the 17th International Conference on Coastal Engineering, pp. 157–172.
Meseguer, A., Guanche, R., 2019. Wind turbine aerodynamics scale-modeling for floating offshore wind platform testing. J. Wind Eng. Ind. Aerod. 186, 49–57.
Molins, C., Trubat, P., Gironella, X., Campos, A., 2015. Design optimization for a truncated catenary mooring system for scale model test. J. Mar. Sci. Eng. 3, 1362–1381.
Muller, K., et al., 2014. Improved tank test procedures for scaled floating offshore wind turbines. s.l. In: Proceedings of the International Wind Engineering Conference, IWEC 2014.
Nielsen, F., Hanson, T., Skaare, B., 2006. Integrated dynamic analysis of floating offshore wind turbines. Hamburg (Germany). In: Proceedings of the 25th International Conference on Offshore Mechanics and Arctic Engineering. OMAE, pp. 671–679.

Otter, A., et al., 2022. A review of modelling techniques for floating offshore wind turbines. Wind Energy 25, 831–857.
Pires, O., et al., 2020. Inclusion of rotor moments in scaled wave tank test of a floating wind turbine using SiL hybrid method. s.l. J. Phys. Conf., 032048
RP-C205, D. N. V. G. L., 2017. Environmental Conditions and Environmental Loads - Recommended Practice. s.l., s.n.
Ruzzo, C., et al., 2016. Progress on the experimental set-up for the testing of a floating offshore wind turbine scaled model in a field site. Wind Eng. 40 (5), 455–467.
Sarmiento, J., et al., 2019. Experimental modelling of a multi-use floating platform for wave and wind energy harvesting. Ocean. Eng. 173, 761–773.
Sauder, T., et al., 2016. Real-time Hybrid Model Testing of a Braceless Semi-submersible Wind Turbine. Part I: the Hybrid Approach. s.l., s.n.
Somoano, M., Battistella, T., Fernández-Ruano, S., Guanche, R., 2021a. Uncertainties assessment in real-time hybrid model for ocean basin testing of a floating offshore wind turbine. s.l. J. Phys. Conf., 012036
Somoano, M., et al., 2021b. Influence of turbulence models on the dynamic response of a semi-submersible floating offshore wind platform. Ocean. Eng. 237, 109629.
Somoano, M., Blanco, D., Rodríguez-Luis, A., Guanche, R., 2022. *Experimental analysis of mooring and power cable dynamics when using elastic string models.* Hamburg (Germany). In: Proceedings of the 41st International Conference on Offshore Mechanics and Arctic Engineering - OMAE, V008T09A044.
Somoano, M., Rodríguez-Luis, A., Blanco, D., Guanche, R., 2024. Effect of bathymetry irregularities on the energy dissipation of a mooring line. Ocean. Eng., 116932
Stansberg, C.T., et al., 2004. Model Testing for Ultradeep Waters. s.l., s.n, pp. 1153–1161.
Stansberg, C.T., Oritsland, O., Ormberg, H., 2001. Challenges in Deep Water Experiments: Hybrid Approach. Rio de Janeiro, Brazil, s.n.
Urban, A.M., Guanche, R., 2019. Wind turbine aerodynamics scale-modeling for floating offshore wind platform testing. J. Wind Eng. Ind. Aerod. 186, 49–57.
Vigara, F., et al., 2019. *COREWIND D1.2: Design Load Basis,* s.l.: ESTEYCO, COBRA, INNOSEA, JDR, UPC, FIHAC, UL INT GMBH.
Viselli, A.M., Goupee, A.J., Dagher, H.J., 2015. Model test of a 1:8-scale floating wind turbine offshore in the Gulf of Maine. J. Offshore Mech. Arctic Eng. 137.
Wang, S., Xing, Y., Karuvathil, A., Gaidai, O., 2023. A comparison study of power performance and extreme load effects of large 10-MW offshore wind turbines. IET Renew. Power Gener. 17, 2195–2214.
Zhang, H., et al., 2012. Investigation on optimization design of an equivalent water depth truncated mooring system based on INSGA-II. J. Mar. Sci. Appl. 11, 208–215.
Zhang, H.M., Huang, S.H., Guan, W.B., 2014. Optimal design of equivalent water depth truncated mooring system based on baton pattern simulated annealing algorithm. China Ocean Eng. 28, 67–80.